STANFORD
AERONAUTICS &
ASTRONAUTICS

Transition in the Jet Created by an Impulsively Started Point Force

Brian Cantwell
Stanford University
June 2, 2025

STANFORD
AERONAUTICS &
ASTRONAUTICS

The jet created by an impulsively started point force

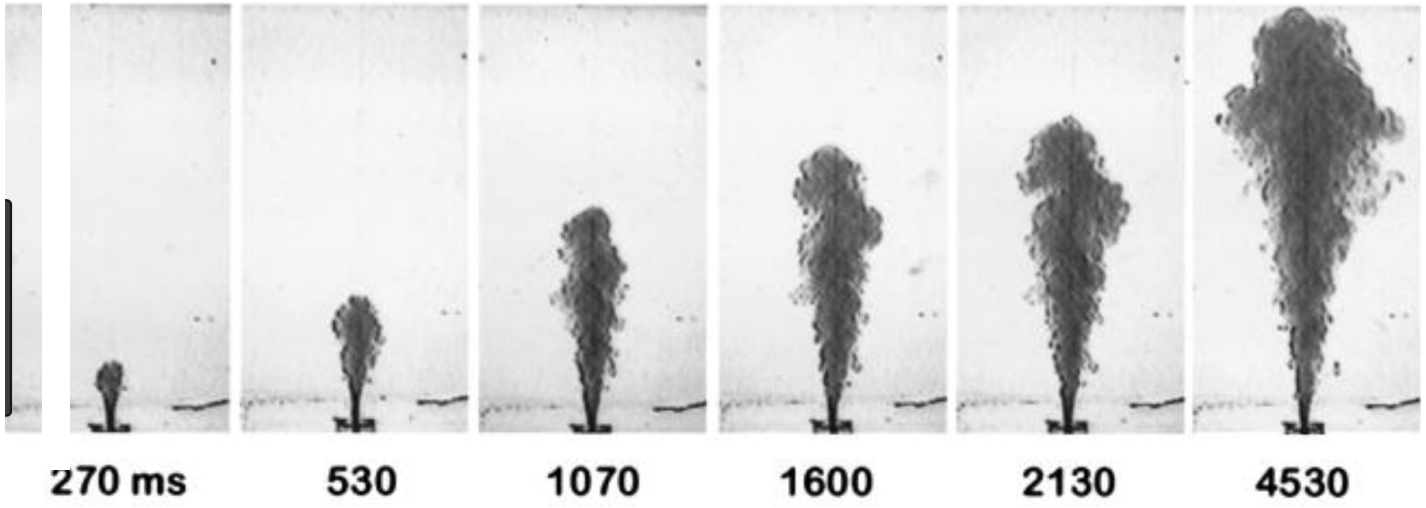

The usual situation is one where the jet is created by the flow of viscous fluid from a tube.

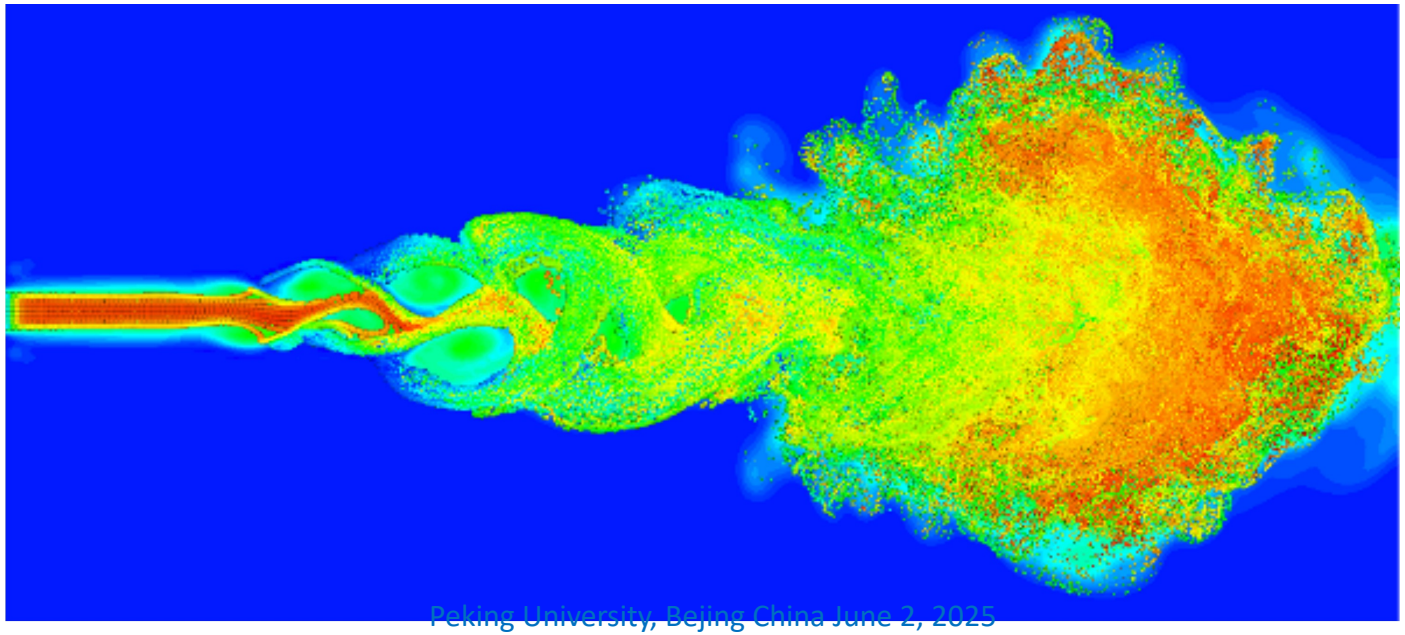

That is <u>not</u> quite the problem we are looking at. Our focus is on the jet produced by a point (zero length scale) force.

STANFORD
AERONAUTICS &
ASTRONAUTICS

Problem definition

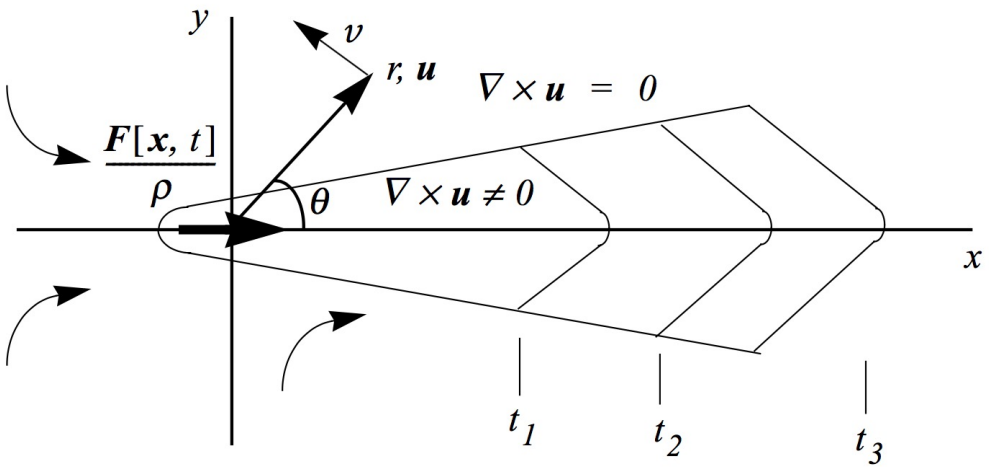

Fig. 11.4. Schematic of the unsteady propagation of a started jet. The boundary schematically delineates the regions of rotational and irrotational flow.

$$\frac{\boldsymbol{F}[\boldsymbol{x},t]}{\rho} = \frac{J}{\rho} h[t]\delta[x]\delta[y]\delta[z]\,\hat{\mathbf{i}}$$

$$h[t] = \begin{cases} 0, & t < 0 \\ 1, & t > 0 \end{cases}$$

$\delta[x]$ is the Dirac delta function

J is the amplitude of the force

Impulse integral

$$\int_V \boldsymbol{u}[\boldsymbol{x},t]\,dx = \frac{2}{3}\left(\frac{J}{\rho}\right) t\,\hat{\mathbf{i}}$$

Much of the material presented can be found in my Text; *Introduction to Symmetry Analysis.*

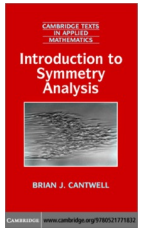

STANFORD
AERONAUTICS &
ASTRONAUTICS

Governing equations

Equations of motion in spherical polar coordinates

$$\frac{1}{r}\frac{\partial(r^2 u)}{\partial r} + \frac{1}{\sin\theta}\frac{\partial(v\sin\theta)}{\partial\theta} = 0, \qquad \text{(continuity)},$$

$$\frac{\partial(rv)}{\partial r} - \frac{\partial u}{\partial\theta} = r\omega \qquad \text{(vorticity)},$$

$$\frac{\partial(r\omega)}{\partial t} + \frac{\partial(ru\omega)}{\partial r} + \frac{\partial(v\omega)}{\partial\theta} = \nu\left(\frac{1}{r}\frac{\partial}{\partial\theta}\left(\frac{1}{\sin\theta}\frac{\partial(\omega\sin\theta)}{\partial\theta}\right) + \frac{\partial^2(r\omega)}{\partial r^2}\right)$$

(momentum).

Express the velocities in terms of the Stokes stream function

$$u = \frac{1}{r^2\sin\theta}\frac{\partial\psi}{\partial\theta}, \qquad v = \frac{-1}{\sin\theta}\frac{\partial\psi}{\partial r}.$$

Equations for particle paths

$$\frac{dr}{dt} = u[r,\theta,t], \qquad \frac{d\theta}{dt} = \frac{v[r,\theta,t]}{r},$$

The problem is invariant under the dilation group of the NS equations

$$\tilde{x}^i = e^a x^i, \qquad \tilde{t} = e^{2a} t,$$

$$\tilde{u}^i = e^{-a} u^i, \qquad \frac{\tilde{p}}{\rho} = e^{-2a} \frac{p}{\rho},$$

$$\tilde{\omega} = e^{-2a} \omega, \qquad \tilde{\psi} = e^a \psi.$$

In spherical polar coordinates the transformation of the spatial coordinates is

$$\tilde{r} = e^a r \qquad \tilde{\theta} = \theta$$

The impulse integral is invariant

$$\int_V \tilde{\boldsymbol{u}}\, d\tilde{\boldsymbol{x}} = \frac{2}{3}\left(\frac{J}{\rho}\right)\tilde{t} \Rightarrow e^{2a}\int_V \boldsymbol{u}\, d\boldsymbol{x} = e^{2a}\frac{2}{3}\left(\frac{J}{\rho}\right)t$$

$$\Rightarrow \int_V \boldsymbol{u}\, d\boldsymbol{x} = \frac{2}{3}\left(\frac{J}{\rho}\right)t.$$

Only if the force that generates the flow has no length scale, are all boundaries of the flow invariant. In other words, there must be no jet tube.

The natural definition of the Reynolds number is

$$Re = \frac{(J/\rho)^{1/2}}{\nu}$$

$$\frac{\hat{J}}{\rho} = \frac{L^4}{T^2}, \quad k = \frac{1}{2}$$

independent of space and time.

STANFORD AERONAUTICS & ASTRONAUTICS

Characteristic equations

$$\frac{dr}{r} = \frac{d\theta}{0} = \frac{dt}{2t} = \frac{du}{-u} = \frac{dv}{-v} = \frac{d(p/\rho)}{-2p/\rho} = \frac{d\omega}{-2\omega} = \frac{d\psi}{\psi}.$$

All the relevant similarity variables are generated as integrals of the characteristic equations.

$$\xi = r/(\nu t)^{1/2},$$
$$\theta = \theta,$$
$$U[\xi,\theta] = \frac{ut^{1/2}}{\nu^{1/2}},$$
$$V[\xi,\theta] = \frac{vt^{1/2}}{\nu^{1/2}},$$
$$P[\xi] = \left(\frac{p}{\rho}\right)\frac{t}{\nu},$$
$$\Omega[\xi,\theta] = \omega t,$$
$$\Psi[\xi,\theta] = \frac{\psi}{\nu^{3/2}t^{1/2}}.$$

STANFORD AERONAUTICS & ASTRONAUTICS

Substitute the similarity variables into the equations of motion

$$\frac{1}{\xi}\frac{\partial(\xi^2 U)}{\partial \xi} + \frac{1}{\sin\theta}\frac{\partial(V\sin\theta)}{\partial\theta} = 0 \qquad \text{(continuity)},$$

$$\frac{\partial(\xi V)}{\partial \xi} - \frac{\partial U}{\partial \theta} = \xi\Omega \qquad \text{(vorticity)},$$

$$\frac{\partial}{\partial\xi}\left(\left(U - \frac{\xi}{2}\right)\xi\Omega\right) + \frac{\partial(V\Omega)}{\partial\theta} = \frac{1}{\xi}\frac{\partial}{\partial\theta}\left(\frac{1}{\sin\theta}\frac{\partial(\Omega\sin\theta)}{\partial\theta}\right) + \frac{\partial^2(\xi\Omega)}{\partial\xi^2} \qquad \text{(momentum)},$$

and the self-similar velocities are

$$U = \frac{1}{\xi^2\sin\theta}\frac{\partial\psi}{\partial\theta}, \qquad V = \frac{-1}{\sin\theta}\frac{\partial\psi}{\partial\xi}.$$

The particle path equations (11.83) become

$$\frac{\partial\xi}{d\tau} = U[\xi,\ \theta; Re] - \frac{\xi}{2}, \qquad \frac{d\theta}{d\tau} = \frac{V[\xi,\ \theta;\ Re]}{\xi},$$

where $\tau = \ln[t]$.

The particle path equations form an autonomous pair of 1st order ODEs with the jet Reynolds number as a parameter.

STANFORD
AERONAUTICS &
ASTRONAUTICS

The geometry of 2D and 3D linear flows

STANFORD
AERONAUTICS &
ASTRONAUTICS

Instantaneous velocity vector field in the wake of a circular cylinder as seen by two observers.

Notice the critical points defining the geometry of the flow pattern

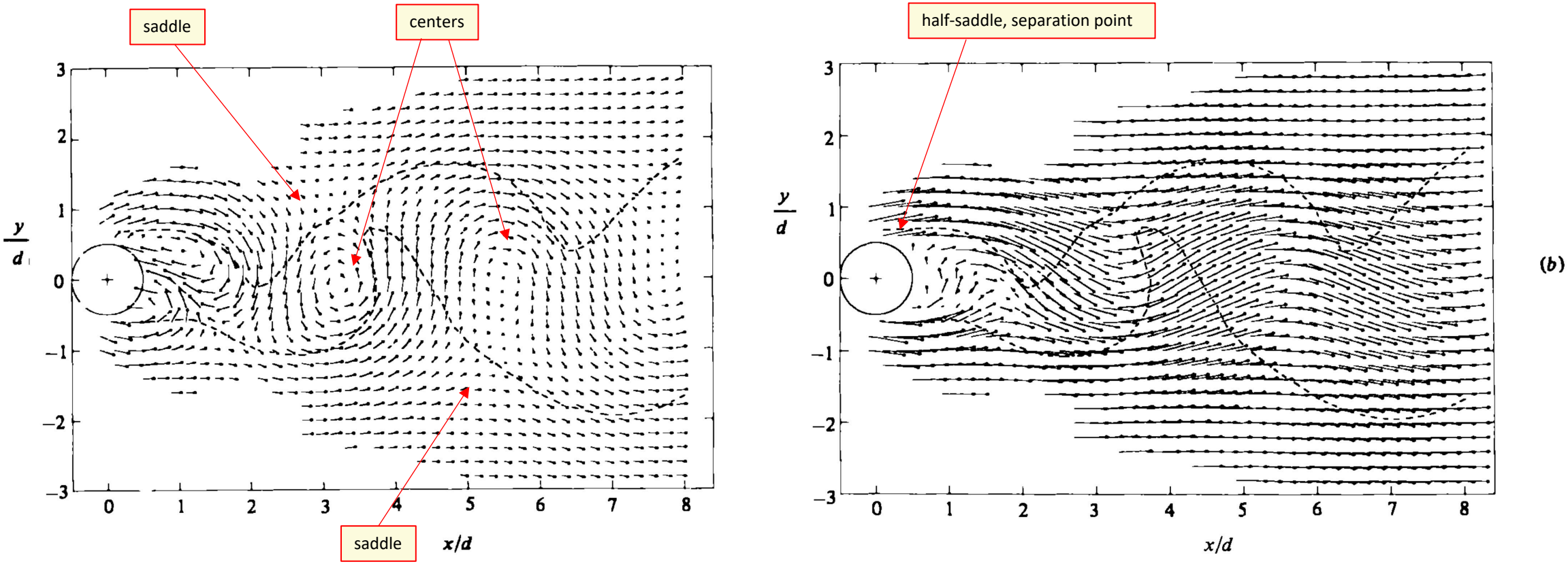

FIGURE 20. Interpolated velocity field at constant phase (7, 15) over 8 diameters of the wake as viewed from a frame of reference (*a*) moving downstream at $0.755u_\infty$, (*b*) fixed with respect to the cylinder. Dashed line is contour $\langle\gamma\rangle = 0.5$ from figure 23(*b*).

The Particle Path Equations

The trajectory of a fluid particle in a three-dimensional unsteady flow is governed by the system of first order ODEs,

$$\frac{dx^1}{dt} = U^1(\mathbf{x}, t) \qquad \frac{dx^2}{dt} = U^2(\mathbf{x}, t) \qquad \frac{dx^3}{dt} = U^3(\mathbf{x}, t)$$

At a given instant in time, $t = t_{fixed}$ the velocity field is frozen and instantaneous streamlines are determined by integrating the autonomous system

$$\frac{dx^1}{ds} = U^1(\mathbf{x}, t_{fixed}) \qquad \frac{dx^2}{ds} = U^2(\mathbf{x}, t_{fixed}) \qquad \frac{dx^3}{ds} = U^3(\mathbf{x}, t_{fixed})$$

where *s* is a pseudotime along an instantaneous streamline. The solution trajectories are

$$x^1 = f^1(\mathbf{x}, s, t_{fixed}) \qquad x^2 = f^2(\mathbf{x}, s, t_{fixed}) \qquad x^3 = f^3(\mathbf{x}, s, t_{fixed})$$

State-space analysis

Very often, the flow field can be completely understood without actually solving the particle path equations. Instead, one looks at critical points, $\mathbf{x_c}$, in the flow field where

$$U^j(\mathbf{x}_c, t_{fixed}) = 0 \qquad j = 1, 2, 3$$

Near a critical point the flow field can be expanded in a Taylor series

$$\frac{dx^j}{dt} = A^j{}_k(x^k - x^k{}_c) + O((x^k - x^k{}_c)^2) + \ldots \qquad j = 1, 2, 3$$

where the matrix of constants is

$$A^j{}_k = \left.\frac{\partial U^j}{\partial x^k}\right|_{\mathbf{x}=\mathbf{x}_c}$$

The geometry of the flow field, ie., the flow pattern in the neighborhood of the critical point, is determined by the eigenvalues of the matrix A^j_k.

Linear Flows in 2-Dimensions

In two dimensions the eigenvalues of A_k^j satisfy the quadratic

$$\lambda^2 + P\lambda + Q = 0,$$

where P and Q are the matrix invariants

$$P = -A_j^j, \qquad Q = \mathrm{Det}(A_k^j).$$

The eigenvalues are

$$\lambda = -\frac{P}{2} \pm \frac{1}{2}\sqrt{P^2 - 4Q},$$

and the character of the local flow is determined by the quadratic discriminant

$$D = Q - \frac{P^2}{4}.$$

If $D > 0$, the eigenvalues are complex and a spiraling motion can be expected. Depending on the sign of P, the spiral may be stable or unstable. If $D < 0$, the eigenvalues are real and a predominantly straining flow can be expected. In this case the directionality of the local flow is defined by the two eigenvectors of A_k^j. The various possible flow patterns can be summarized on a crossplot of the invariants shown in Figure 3.5.

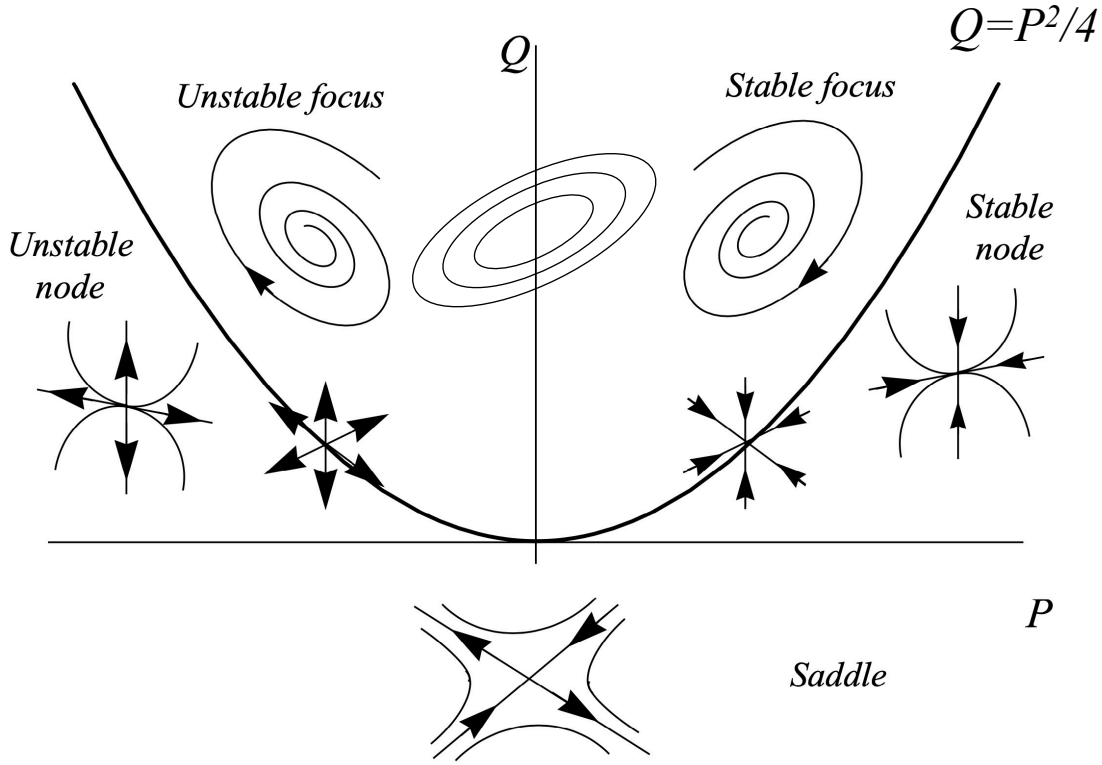

Fig. 3.5. Classification of linear solution trajectories in two dimensions.

Linear Flows in 3 - Dimensions

In three dimensions the eigenvalues of A_k^j satisfy the cubic

$$\lambda^3 + P\lambda^2 + Q\lambda + R = 0,$$

where the invariants are

$$P = -\mathrm{tr}[A] = -A_j^j,$$
$$Q = \tfrac{1}{2}(P^2 - \mathrm{tr}[A^2]) = \tfrac{1}{2}\left(P^2 - A_k^j A_j^k\right),$$
$$R = \tfrac{1}{3}(-P^3 + 3PQ - \mathrm{tr}[A^3]) = \tfrac{1}{3}\left(-P^3 + 3PQ - A_k^j A_m^k A_j^m\right).$$

Any cubic can be simplified as follows. Let

$$\lambda = \alpha - \frac{P}{3}.$$

Then α satisfies

$$\alpha^3 + \hat{Q}\alpha + \hat{R} = 0,$$

where

$$\hat{Q} = Q - \tfrac{1}{3}P^2, \qquad \hat{R} = R - \tfrac{1}{3}PQ + \tfrac{2}{27}P^3.$$

Let

$$a_1 = \left(-\frac{\hat{R}}{2} + \frac{1}{3\sqrt{3}}\left(\hat{Q}^3 + \tfrac{27}{4}\hat{R}^2\right)^{1/2}\right)^{1/3},$$

$$a_2 = \left(-\frac{\hat{R}}{2} - \frac{1}{3\sqrt{3}}\left(\hat{Q}^3 + \tfrac{27}{4}\hat{R}^2\right)^{1/2}\right)^{1/3}$$

The real solution is expressed as

$$\alpha_1 = a_1 + a_2,$$

and the complex (or remaining real) solutions are

$$\alpha_2 = -\tfrac{1}{2}(a_1 + a_2) + \frac{i\sqrt{3}}{2}(a_1 - a_2),$$

$$\alpha_3 = -\tfrac{1}{2}(a_1 + a_2) - \frac{i\sqrt{3}}{2}(a_1 - a_2).$$

Solving for the eigenvalues leads to the cubic discriminant.

$$D = \tfrac{27}{4}R^2 + \left(P^3 - \tfrac{9}{2}PQ\right)R + Q^2\left(Q - \tfrac{1}{4}P^2\right).$$

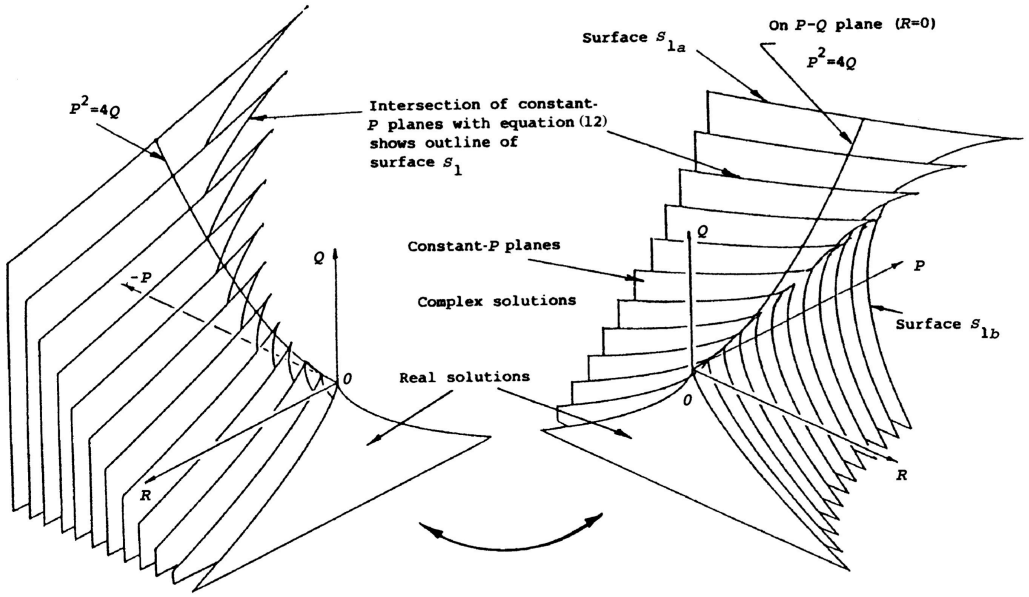

Fig. 3.8. The Cardano surface dividing real and complex eigenvalues in three dimensions (from Reference [3.10]).

Incompressible critical points

3D Discriminant

$$D = \tfrac{27}{4}R^2 + \left(P^3 - \tfrac{9}{2}PQ\right)R + Q^2\left(Q - \tfrac{1}{4}P^2\right)$$

If $P = 0$ $\qquad D = Q^3 + \dfrac{27}{4}R^2$

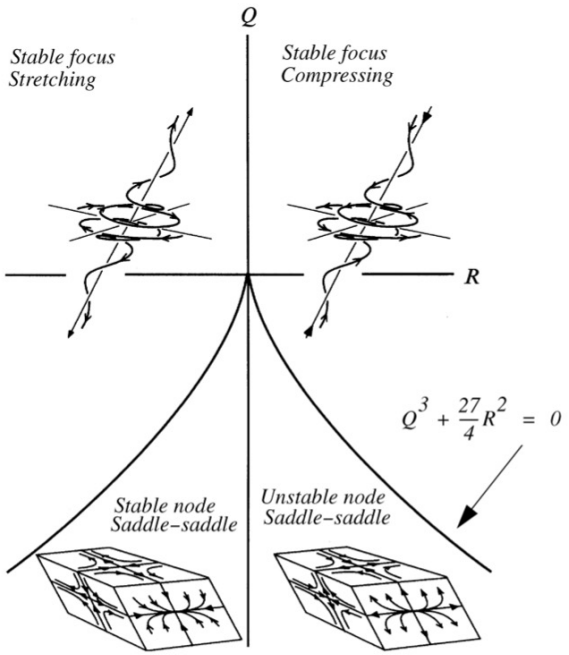

Fig. 3.9. Three-dimensional flow patterns in the plane $P = 0$ (from Reference [3.11]).

The second invariant Q represents a balance between rotation and strain

$$\frac{\partial u^i}{\partial x^j} = \frac{1}{2}\left(\frac{\partial u^i}{\partial x^j} + \frac{\partial u^j}{\partial x^i}\right) + \frac{1}{2}\left(\frac{\partial u^i}{\partial x^j} - \frac{\partial u^j}{\partial x^i}\right)$$

$$A^i_j = S^i_j + W^i_j$$

$$Q = -\frac{1}{2}A^j_k A^k_j = -\frac{1}{2}S^j_k S^k_j - \frac{1}{2}S^j_k W^k_j - \frac{1}{2}W^j_k S^k_j - \frac{1}{2}W^j_k W^k_j$$

$$Q = Q_S + Q_W$$

$$Q_S = -\frac{1}{2}S^j_k S^k_j < 0$$

$$Q_W = -\frac{1}{2}W^j_k W^k_j = \Omega_i \Omega_i > 0$$

$$R = -\frac{1}{3}A^j_k A^k_m A^m_j = -\frac{1}{3}S^j_k S^k_m S^m_j - W^j_k W^k_m S^m_j$$

STANFORD
AERONAUTICS &
ASTRONAUTICS

Particle path field of the impulsively started jet

STANFORD AERONAUTICS & ASTRONAUTICS

Critical points in the vector field of particle paths

The analysis of critical points in the jet uses the theory just developed and for this purpose it is easier to work in Cartesian coordinates.

$$\frac{dx^i}{dt} = u^i(\boldsymbol{x}, t) \Rightarrow \frac{d\xi^i}{d\tau} = U^i[\boldsymbol{\xi}; Re] - \frac{\xi^i}{2}$$

where $\xi^i = x^i/\sqrt{\nu t}$

Expand the particle path field in a Taylor series about the critical point.

$$\frac{d\xi^i}{d\tau} = \left(A^i_j - \frac{1}{2}\delta^i_j\right)\Big|_{\boldsymbol{\xi}=\boldsymbol{\xi}_c} \left(\xi^j - \xi^j_c\right)$$

Relationship between the gradient of the physical and the gradient of the self-similar velocity field

$$a^i_j = \frac{\partial u^i}{\partial x^j} = \frac{1}{t}\frac{\partial U^i}{\partial \xi^j} = \frac{1}{t}A^i_j[\boldsymbol{\xi}]$$

Note that the value of the dimensioned velocity gradient tensor does not depend on J/ρ or ν. Therefore an observer moving at a fixed $\boldsymbol{\xi}$ can use the current value of the velocity gradient as a local clock to determine the global age of the flow, regardless of the flow Reynolds number.

Velocity field gradient and particle path field gradient

$$M_j^i = A_j^i - \tfrac{1}{2}\delta_j^i$$

First invariants

$$P_M = \tfrac{3}{2}, \qquad P_A = 0.$$

Second invariants

$$Q_A = -\tfrac{1}{2}A_k^i A_i^k,$$

$$Q_M = \tfrac{9}{8} - \tfrac{1}{2}M_k^i M_i^k$$

Third invariants

$$R_A = -\tfrac{1}{3}A_k^i A_j^k A_i^j,$$

$$R_M = -\tfrac{1}{3}M_k^i M_j^k M_i^j - \tfrac{3}{2}Q_M + \tfrac{27}{24}$$

Relationship between the invariants of M and A

$$Q_M = Q_A + \tfrac{3}{4},$$

$$R_M = R_A + \tfrac{1}{2}Q_A + \tfrac{1}{8}$$

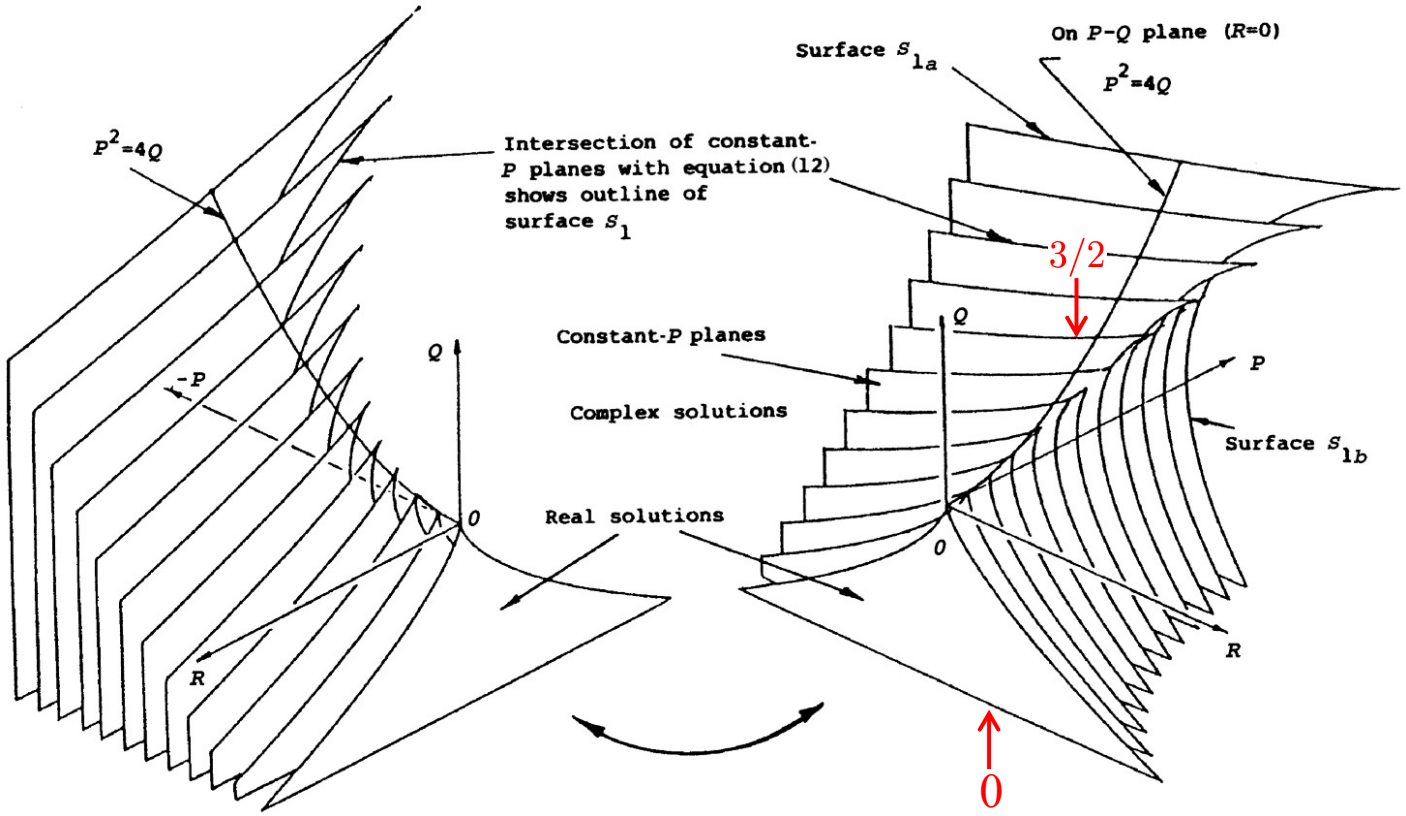

Discriminant of A

$$D_A = Q_A^3 + \tfrac{27}{4}R_A^2$$

Discriminant of M

$$D_M = Q_M^3 + \tfrac{27}{4}R_M^2 + \tfrac{27}{4}R_M\left(\tfrac{1}{2} - Q_M\right) - \tfrac{9}{16}Q_M^2$$

Boundary conditions for the impulsively started jet

$$\xi = r/(\nu t)^{1/2} \qquad \Psi[\xi,\theta] = \frac{\psi}{\nu^{3/2} t^{1/2}}$$

The Limit $\xi \to 0$

$$\psi = \nu r\left(\frac{2\sin^2\theta}{A[Re]-\cos\theta}\right)$$

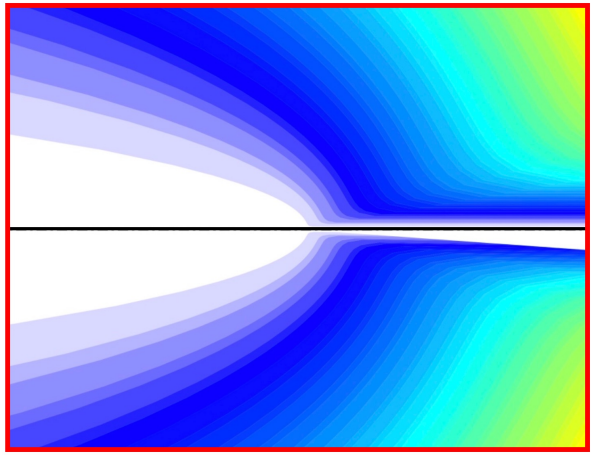

Landau-Squire jet streamline pattern

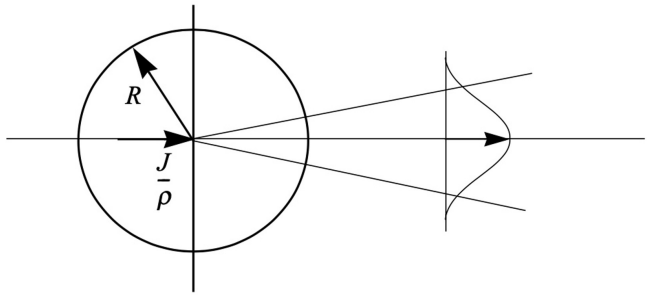

Fig. 11.5. Control volume surrounding the steady round jet.

$$\frac{J}{\rho} = \int_0^\pi (u(u\cos\theta - v\sin\theta) - \left(\frac{\tau_{rr}}{\rho}\cos\theta - \frac{P}{\rho}\cos\theta - \frac{\tau_{r\theta}}{\rho}\sin\theta\right)$$
$$\times 2\pi R^2 \sin\theta\, d\theta.$$

$$\frac{Re^2}{16\pi} = A + \frac{4}{3}\left(\frac{A}{A^2-1}\right) - \frac{A^2}{2}\ln\left(\frac{A+1}{A-1}\right)$$

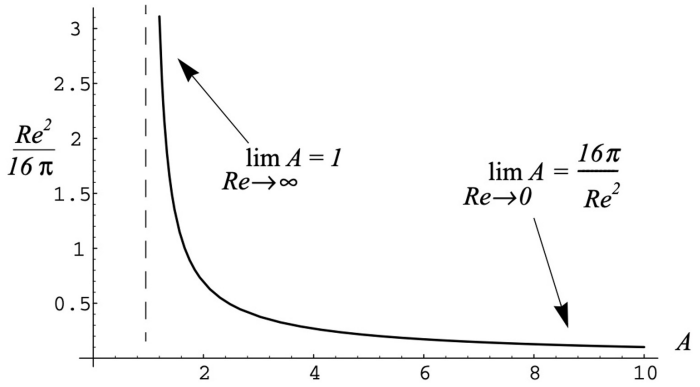

Fig. 11.6. The constant A in the Landau–Squire solution.

Multiply and divide by $(\nu t)^{1/2}$

$$\Psi_0 = \xi\left(\frac{2\sin^2\theta}{A[Re]-\cos\theta}\right).$$

The Limit $\xi \to \infty$

$$\psi = \frac{1}{4\pi}\left(\frac{J}{\rho}t\right)\frac{\sin^2\theta}{r}$$

$r \to \xi\sqrt{\nu t}$ and $J/\rho = Re^2\nu^2$

$$\Psi_\infty = \frac{Re^2}{4\pi}\left(\frac{\sin^2\theta}{\xi}\right).$$

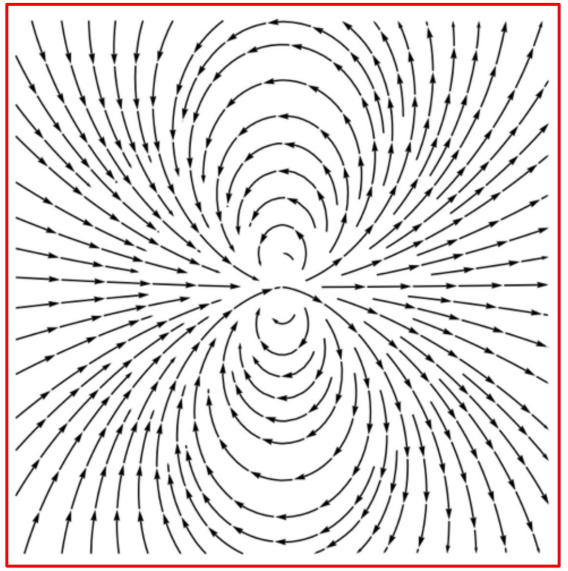

For the axisymmetric flow considered here, the velocity gradient tensor takes the form

$$A_j^i = \begin{bmatrix} \dfrac{\partial U}{\partial \xi} & \dfrac{1}{\xi}\dfrac{\partial U}{\partial \theta} - \dfrac{V}{\xi} & 0 \\ \dfrac{\partial V}{\partial \xi} & \dfrac{1}{\xi}\dfrac{\partial V}{\partial \theta} + \dfrac{U}{\xi} & 0 \\ 0 & 0 & \dfrac{V}{\xi}\cot\theta + \dfrac{U}{\xi} \end{bmatrix}.$$

Given the velocity functions, This equation is evaluated at the critical point and the invariants are computed. Interestingly, it turns out that *often the values of the invariants can be determined without knowing the velocity functions explicitly*. In general, Q, R, ξ_c, and θ_c all depend on Re resulting in the possibility of bifurcation in the phase space of particle paths.

STANFORD AERONAUTICS & ASTRONAUTICS

Particle paths of the Landau-Squire Jet, $\xi \rightarrow 0$

Particle path equations

$$\frac{d\xi}{d\tau} = \frac{2}{\xi}\left(\frac{A^2-1}{(A-\cos\theta)^2} - 1\right) - \frac{\xi}{2}, \qquad \frac{d\theta}{d\tau} = \frac{2\sin\theta}{\xi^2(A-\cos\theta)}$$

The critical point location depends on the Reynolds number

$$(\xi_c, \theta_c) = \left(\frac{2^{3/2}}{(A-1)^{1/2}}, 0\right)$$

Gradients evaluated at the critical point

$$A^i_j = \begin{bmatrix} -\frac{1}{2} & 0 & 0 \\ 0 & \frac{1}{4} & 0 \\ 0 & 0 & \frac{1}{4} \end{bmatrix}, \qquad M^i_j = \begin{bmatrix} -1 & 0 & 0 \\ 0 & -\frac{1}{4} & 0 \\ 0 & 0 & -\frac{1}{4} \end{bmatrix}$$

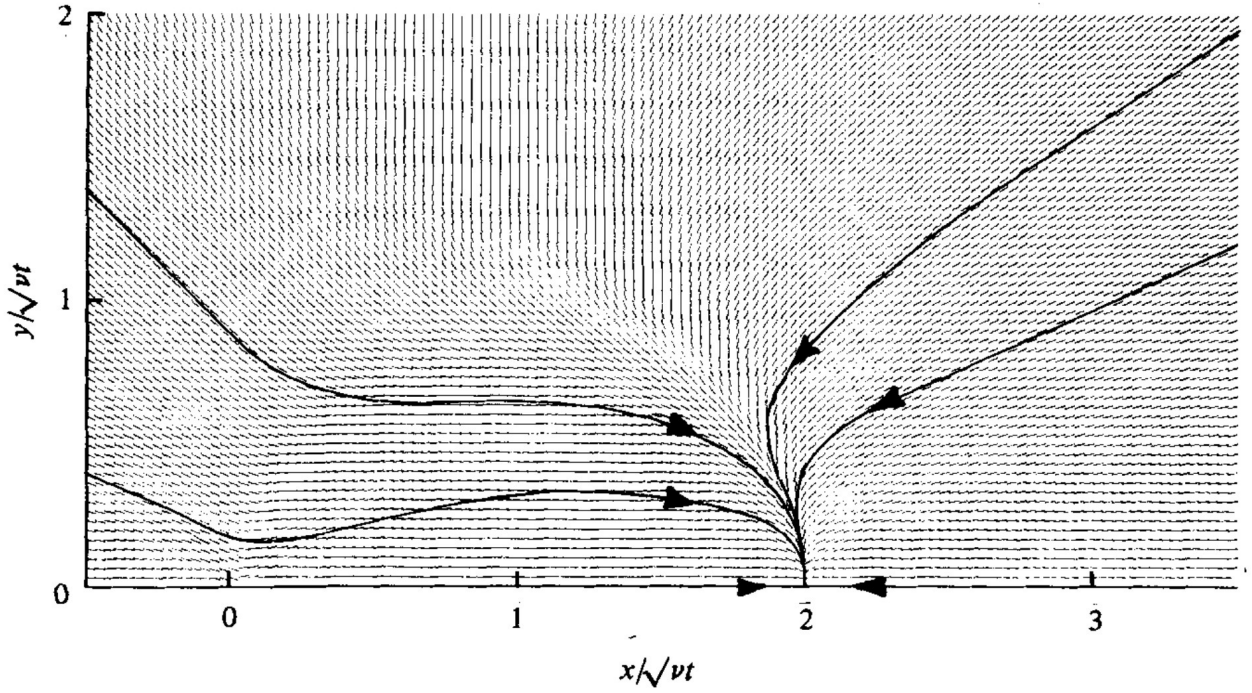

Critical point invariants do not depend on Reynolds number

$$(P_M, Q_M, R_M) = (\tfrac{3}{2}, \tfrac{9}{16}, \tfrac{1}{16})$$

Particle paths of the unsteady dipole, $\xi \rightarrow \infty$

Particle path equations

$$\frac{d\xi}{d\tau} = \frac{Re^2}{2\pi}\frac{\cos\theta}{\xi^3} - \frac{\xi}{2}, \qquad \frac{d\theta}{d\tau} = \frac{Re^2}{2\pi}\frac{\sin\theta}{\xi^4}$$

The critical point location depends on the Reynolds number

$$(\xi_c, \theta_c) = (Re^{1/2}/\pi^{1/4}, 0)$$

Gradients evaluated at the critical point

$$A^i_j = \begin{bmatrix} -\frac{3}{2} & 0 & 0 \\ 0 & \frac{3}{4} & 0 \\ 0 & 0 & \frac{3}{4} \end{bmatrix}, \qquad M^i_j = \begin{bmatrix} -2 & 0 & 0 \\ 0 & \frac{1}{4} & 0 \\ 0 & 0 & \frac{1}{4} \end{bmatrix}$$

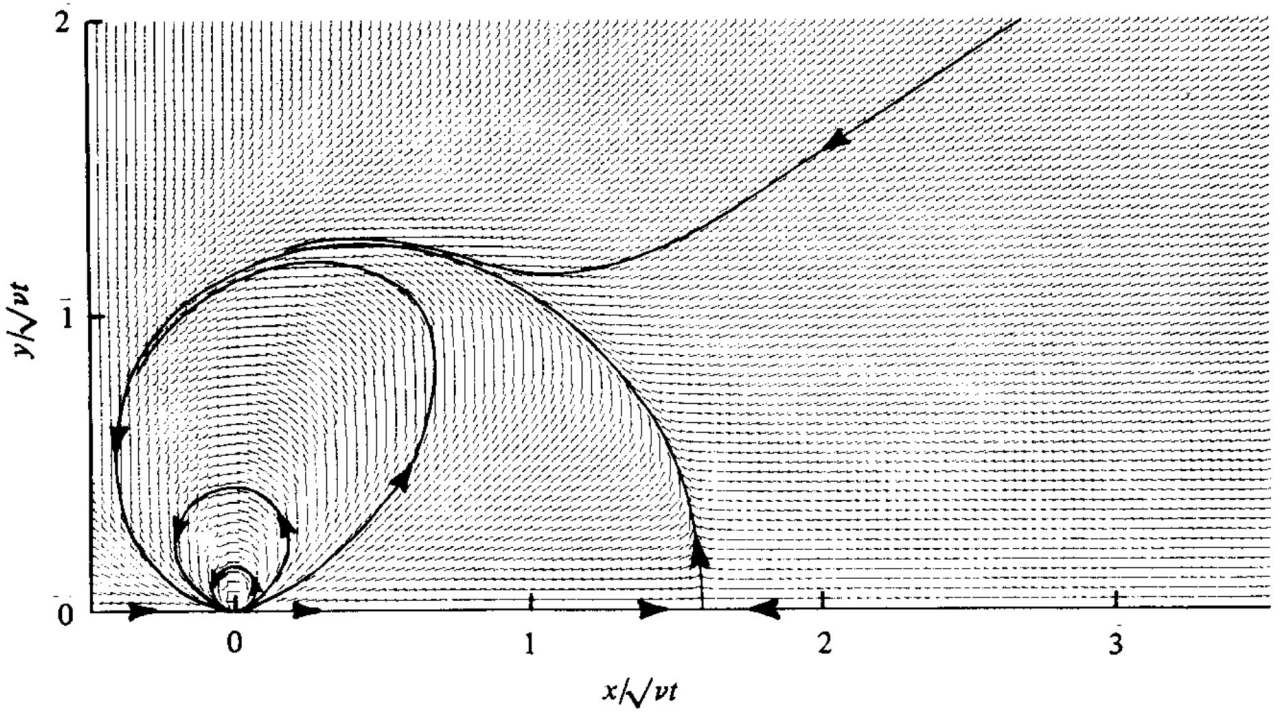

Critical point invariants do not depend on Reynolds number

$$(P_M, Q_M, R_M) = (\tfrac{3}{2}, -\tfrac{15}{16}, \tfrac{1}{8})$$

The Stokes flow limit $Re \to 0$.

In the limit $Re \to 0$.

$$A = 16\pi / Re^2$$

$$\lim_{Re\to 0} \Psi[\xi,\theta] = \frac{Re^2}{16\pi}(\sin^2\theta) g[\xi]$$

$$\lim_{\xi\to 0} g[\xi] = 2\xi, \qquad \lim_{\xi\to\infty} g[\xi] = \frac{4}{\xi}$$

Solve for the vorticity

$$\frac{d}{d\xi}\left(\frac{1}{\xi^2}\frac{d}{d\xi}(\xi g[\xi])\right) = -\frac{f[\xi]}{8}$$

$$\xi^2 f_{\xi\xi} + 2\xi\left(1 + \frac{\xi^2}{4}\right) f_\xi + (\xi^2 - 2) f = 0.$$

Stokes stream function

$$\lim_{Re\to 0} \Psi[\xi,\theta] = \frac{Re^2}{16\pi} \sin^2\theta \left(2\xi - \frac{4}{\sqrt{\pi}} e^{-\xi^2/4} - \left(2\xi - \frac{4}{\xi}\right) \text{erf}\,[\xi/2]\right).$$

Stream Function Re = 4

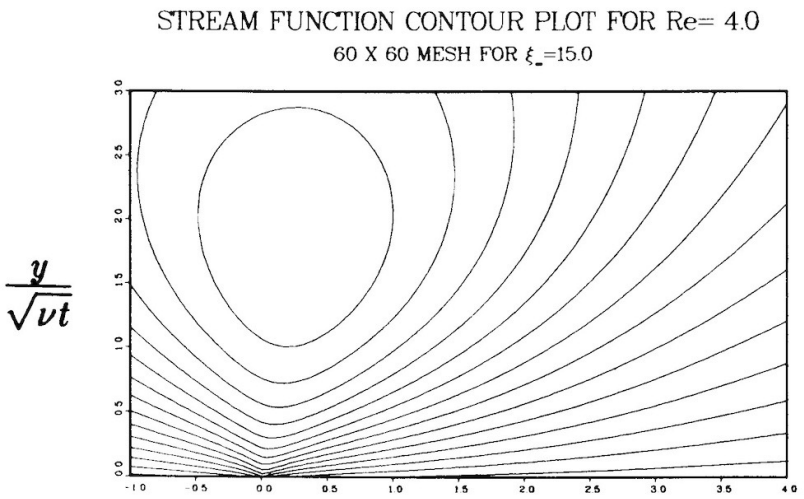

Vorticity Re = 4

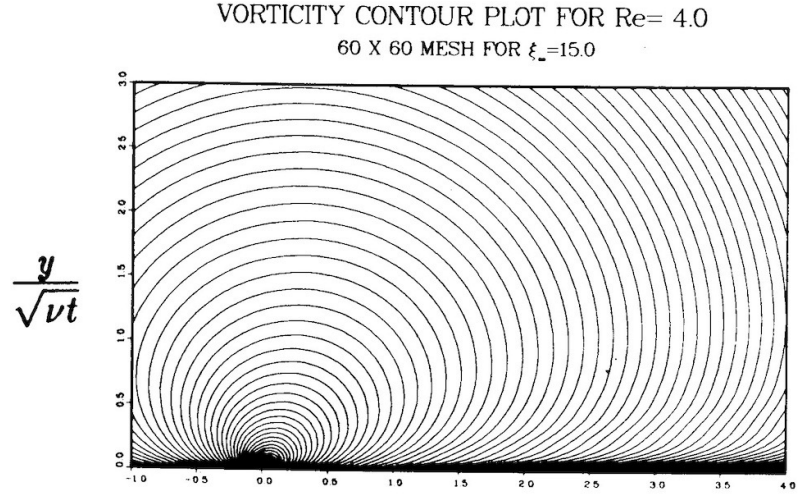

STANFORD AERONAUTICS & ASTRONAUTICS

Particle paths in the low Reynolds number jet

Particle path equations

$$\frac{d\xi}{d\tau} = \frac{Re^2}{2\pi}\frac{\cos\theta}{\xi^2}\left(\frac{\xi}{2} - \frac{1}{\sqrt{\pi}}e^{-\xi^2/4} - \left(\frac{\xi}{2} - \frac{1}{\xi}\right)\mathrm{erf}\,[\xi/2]\right) - \frac{\xi}{2}$$

$$\frac{d\theta}{d\tau} = -\frac{Re^2}{4\pi}\frac{\sin\theta}{\xi^2}\left(\frac{1}{2} + \frac{1}{\xi\sqrt{\pi}}e^{-\xi^2/4} - \left(\frac{1}{2} + \frac{1}{\xi^2}\right)\mathrm{erf}\,[\xi/2]\right).$$

Zeros of the θ-equation occur at $\theta = 0,\ \pi$ for all ξ and at $\xi = 1.7633$ for all θ and do not depend on the Reynolds number.

Zeros of the radial equation do depend on Reynolds number.

$$Re^2 = \frac{\pi\xi_c^3}{\left(\frac{\xi_c}{2} - \frac{1}{\sqrt{\pi}}e^{-\xi_c^2/4} - \left(\frac{\xi_c}{2} - \frac{1}{\xi_c}\right)\mathrm{erf}\,[\xi_c/2]\right)\cos\theta}$$

Particle paths in the Stokes jet at 3 Reynolds numbers

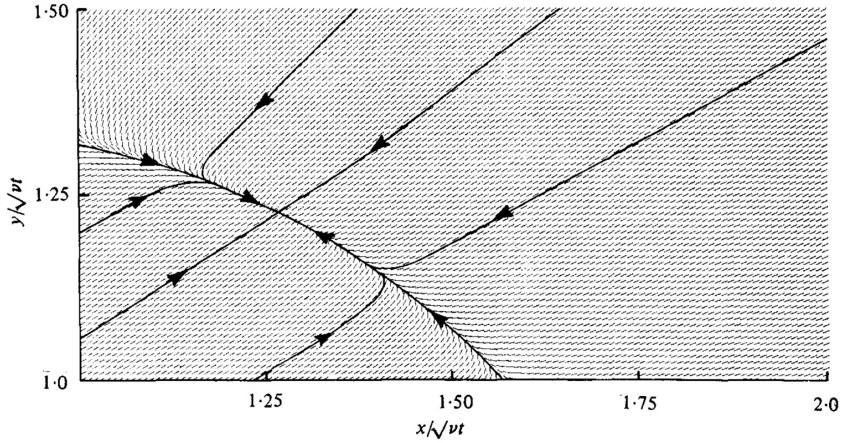

The nature of transition in the jet created by an impulsive point force is a sequence of bifurcations in the phase portrait of particle paths in similarity coordinates.

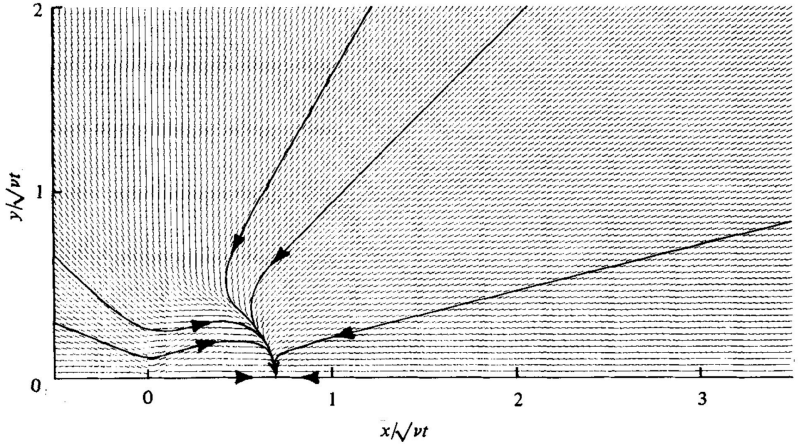

Re = 2

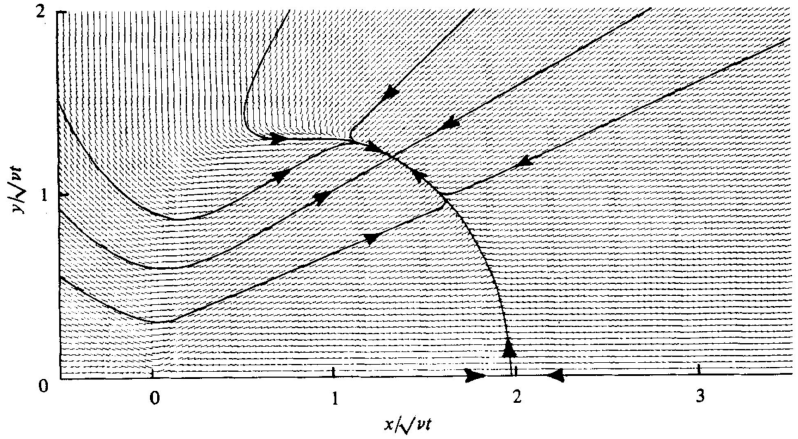

Re = 8

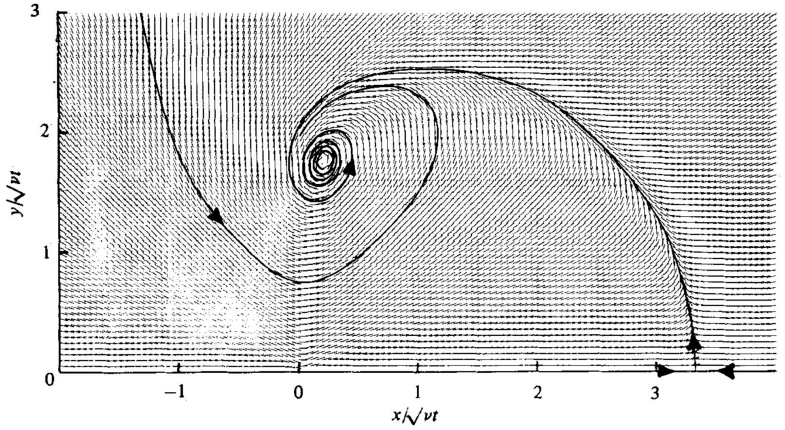

Re = 20

Transition in the space of invariants Q_M and R_M

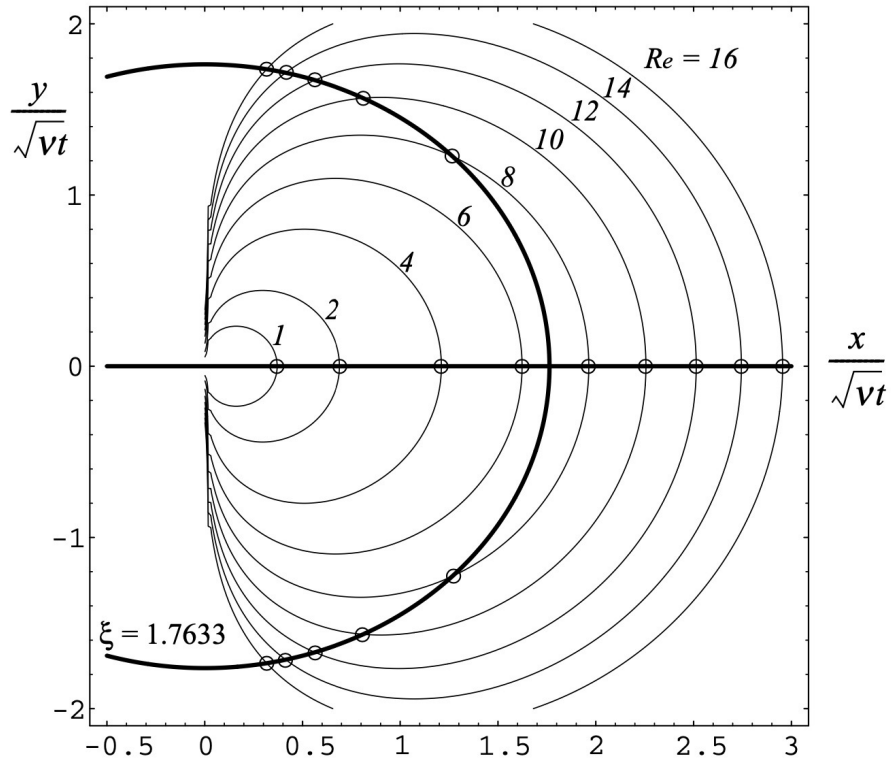

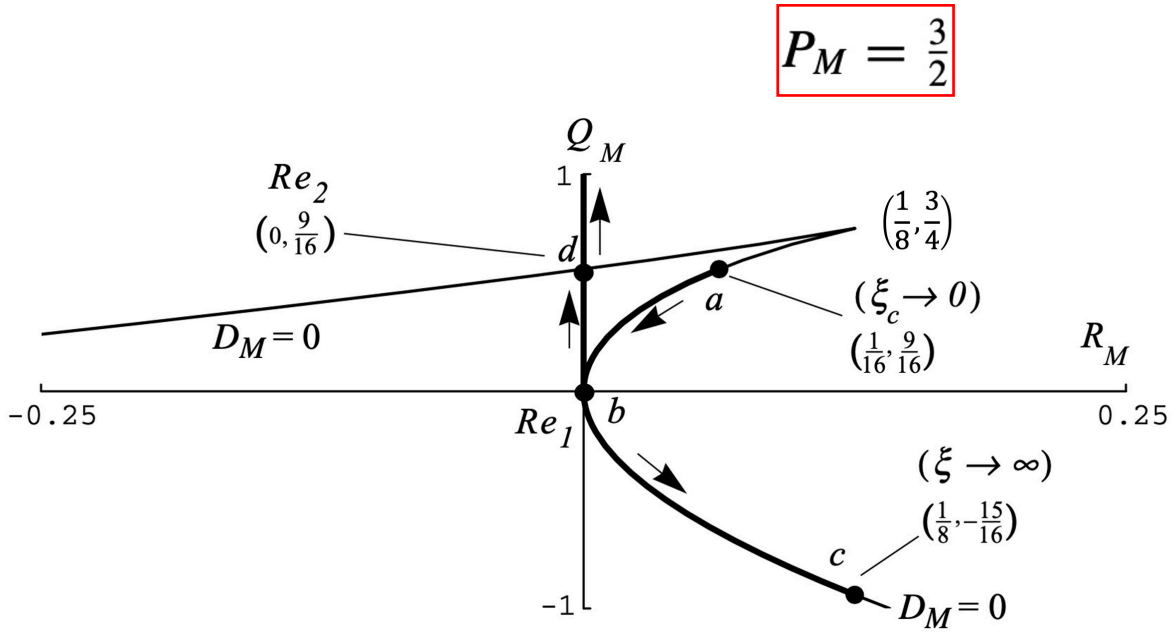

Fig. 11.7. Critical-point locations at several Reynolds numbers for the Stokes jet. The circle has radius 1.7633.

STANFORD AERONAUTICS & ASTRONAUTICS

Another view of particle paths in the Stokes jet.

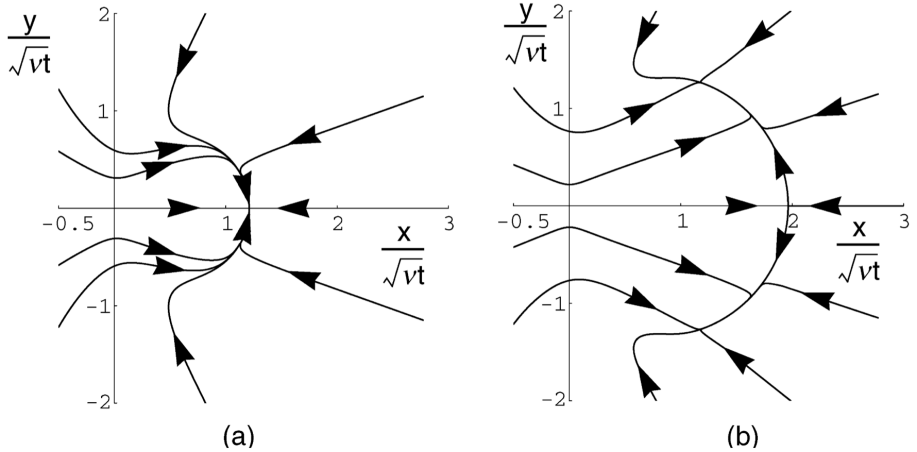

Fig. 11.9. Particle paths for the impulsively started creeping jet at (a) $Re = 4$ and (b) $Re = 8$.

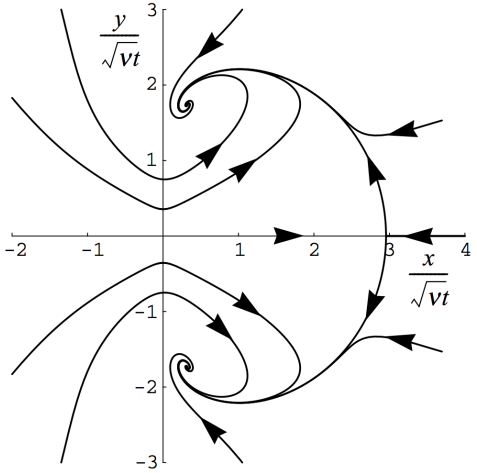

Fig. 11.10. Particle paths for the impulsively started creeping jet at $Re = 16$.

The impulsively started round jet undergoes a bifurcation in the phase portrait of particle paths. For the Stokes solution, the first transition to an off-axis stable node occurs at Re = 6.7806 and the onset of a starting occurs at Re=10.09089.

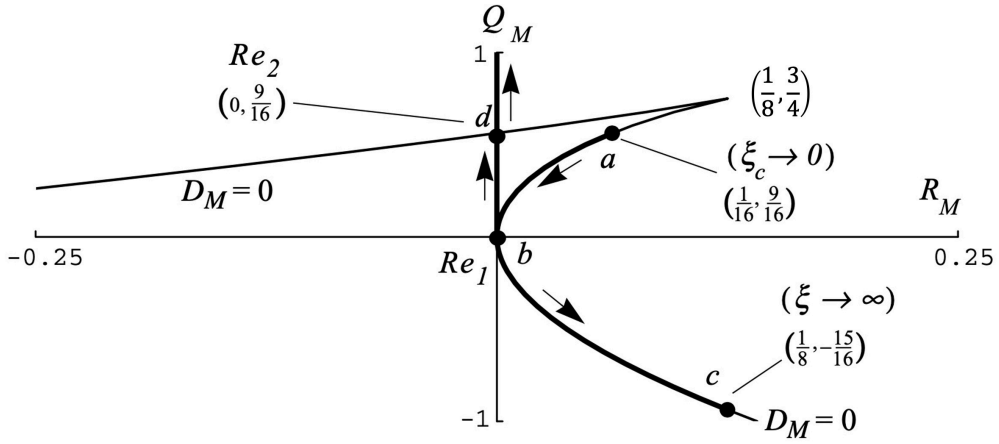

The nonlinear axisymmetric jet follows the same path in the space of Q_M and R_M invariants.

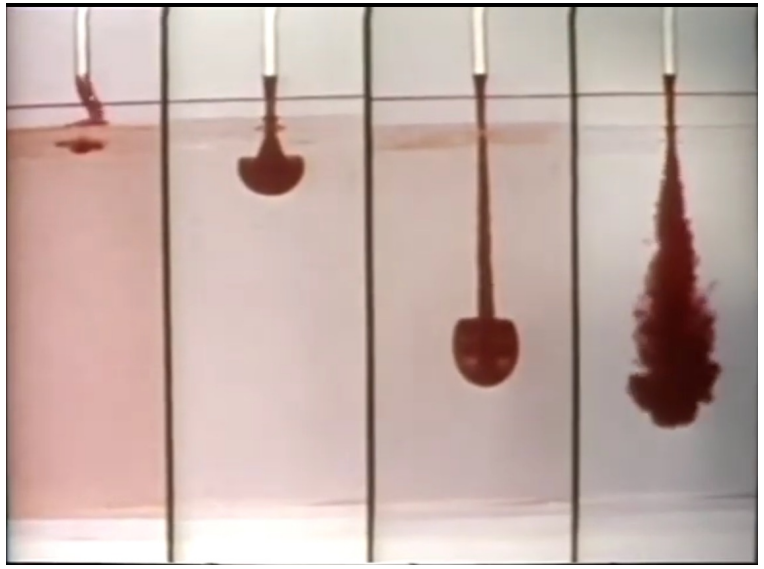

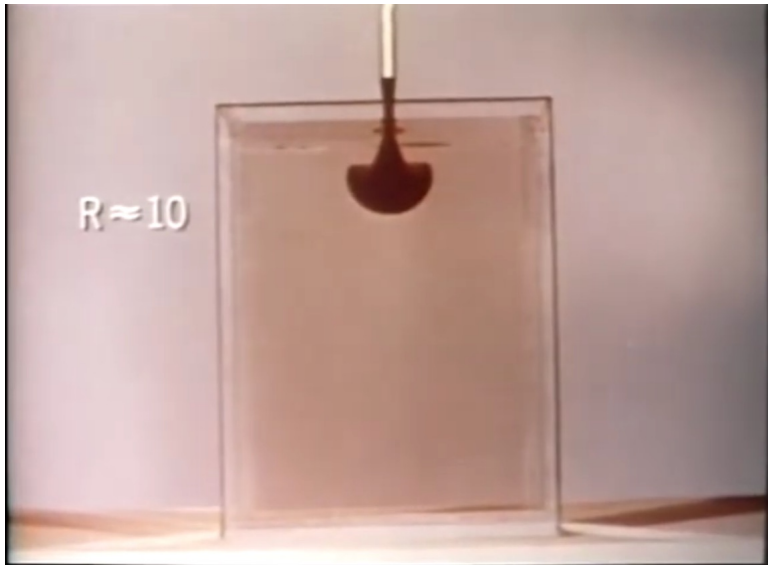

https://web.mit.edu/hml/ncfmf.html

Streamlines, vorticity and particle paths for the nonlinear round jet

Re=4

Re=6

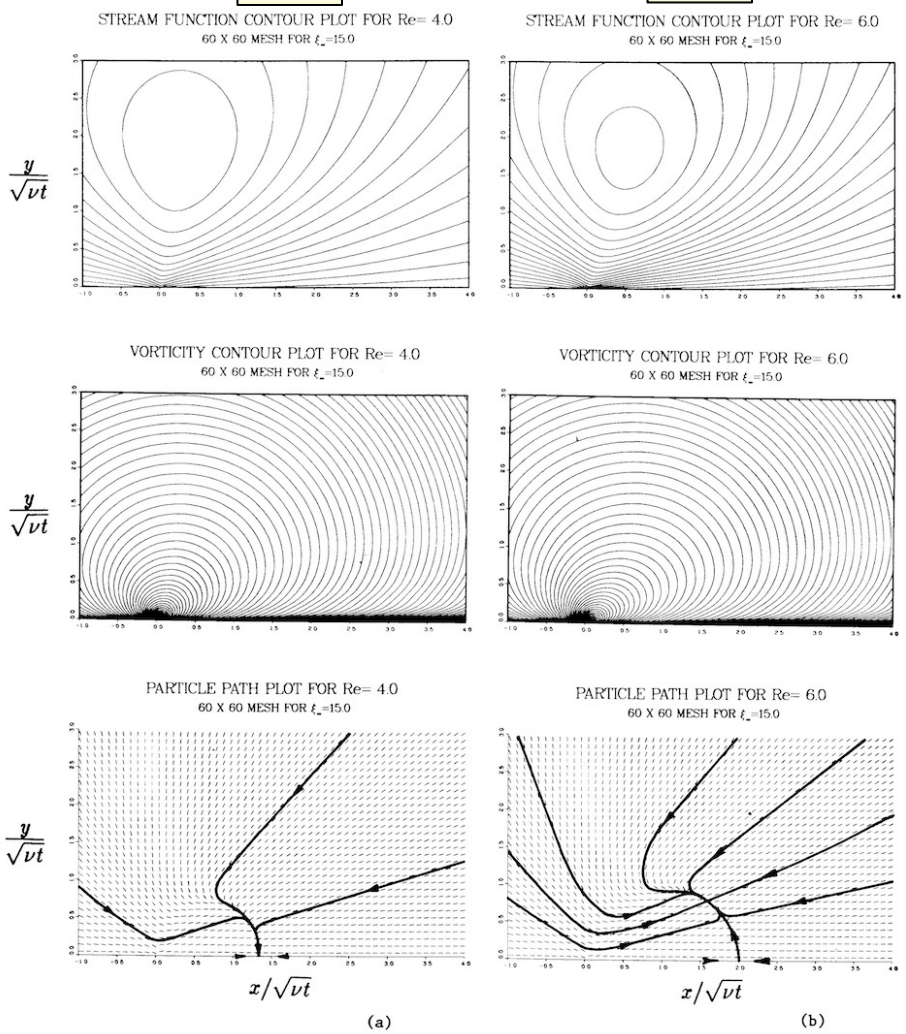

Figure 4. Computed solutions for the round jet at a) $Re = 4.0$ and b) $Re = 6.0$. Quantities displayed are self–similar stream function, vorticity and particle paths.

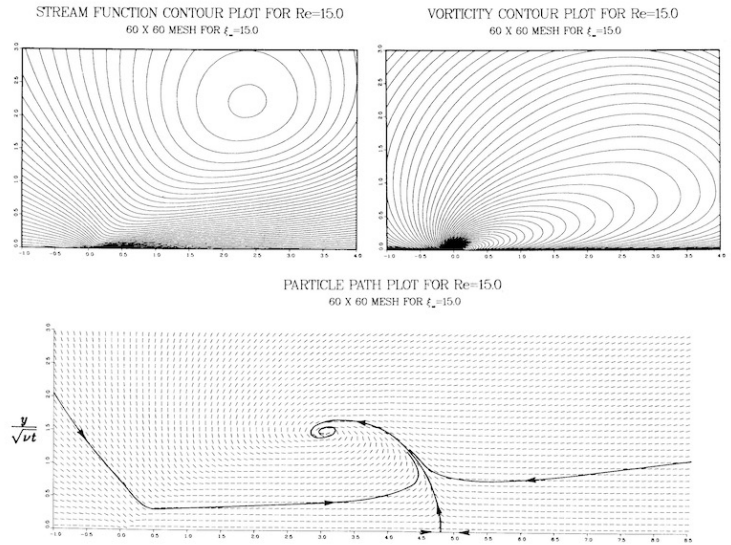

Re=15

Figure 5. Computed solution for the round jet at $Re = 15.0$.

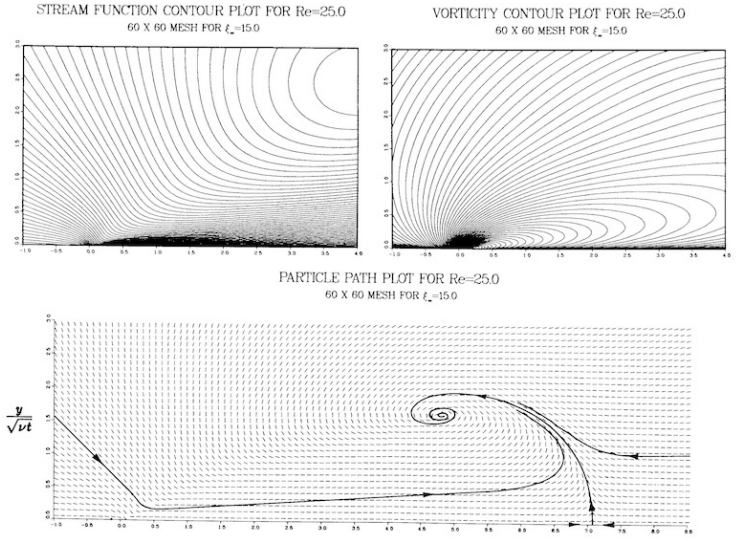

Re=25

Figure 6. Computed solution for the round jet at $Re = 25.0$.

Invariance of the vector field of particle paths relative to a moving observer

The Navier Stokes equations are invariant under a non-uniform translation group.

In the round jet all length scales vary in proportion to $(\nu t)^{1/2}$.

Consider an observer who translates according to this time scale.

$$\tilde{x}^j = x^j + \alpha^j (\nu t)^{1/2},$$
$$\tilde{t} = t,$$
$$\tilde{u}^i = u^i + \frac{\alpha^i}{2} \nu^{1/2} t^{-1/2},$$
$$\frac{\tilde{p}}{\rho} = \frac{p}{\rho} + x^k \frac{\alpha^k}{4} \nu^{1/2} t^{-3/2}, \quad \text{sum over } k$$

where the α^i determine the rate at which the observer moves in each direction.

In similarity coordinates, the position and velocity transformations become the following.

$$\tilde{\xi}^j = \xi^j + \alpha^j,$$
$$\tilde{U}^i = U^i + \frac{\alpha^i}{2}$$

The right sides of the particle path equations are invariant.

$$\frac{d\xi^i}{d\tau} = U^i[\boldsymbol{\xi}] - \frac{1}{2}\xi^i$$

$$\tilde{U}^i - \frac{1}{2}\tilde{\xi}^i = \left(U^i + \frac{\alpha^i}{2}\right) - \frac{1}{2}(\xi^j + \alpha^j) = U^i - \frac{1}{2}\xi^j$$

Transition in the impulsively started jet culminates in the onset of a starting vortex

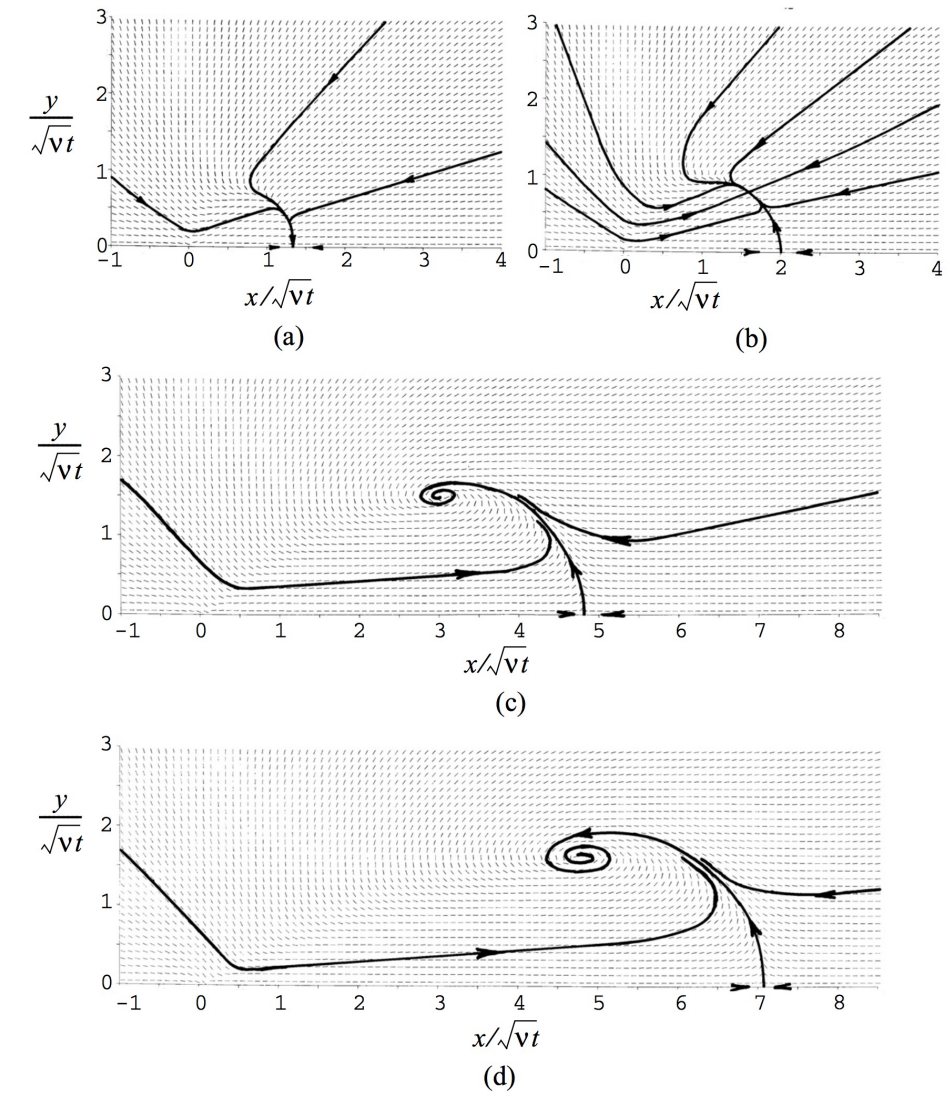

Fig. 11.11. Numerically computed particle paths in the round jet at Reynolds numbers (a) $Re = 4$, (b) $Re = 6$, (c) $Re = 15$, (d) $Re = 25$.

For the numerically computed nonlinear solution, the first transition to an off-axis stable node occurs at Re = 5.5 and the onset of a starting occurs at Re=7.545.

Mixing of Material Lines at 3 Reynolds numbers

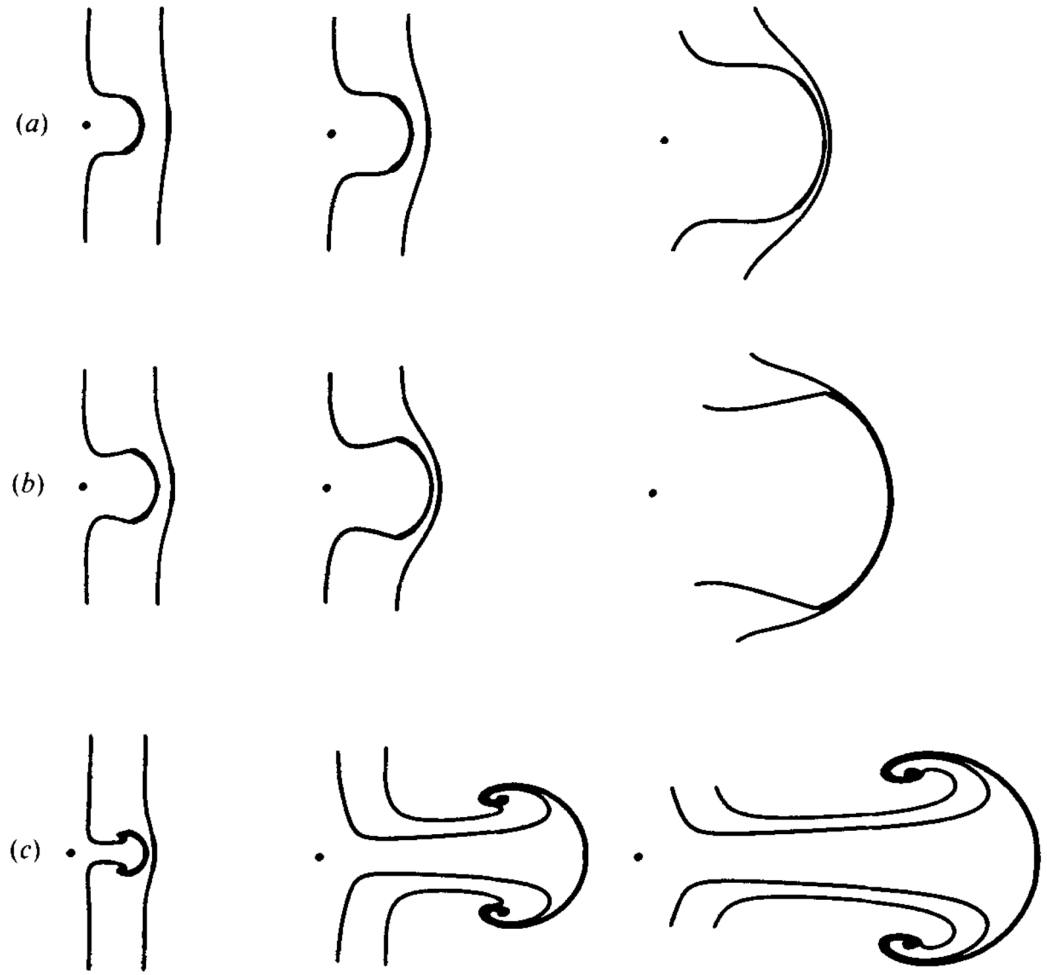

FIGURE 8. Distortion of timelines in physical coordinates under the action of the nonlinear round jet at (*a*) $Re = 4$, (*b*) $Re = 6$, (*c*) $Re = 30$. Time increases from left to right.

STANFORD
AERONAUTICS &
ASTRONAUTICS

Elliptic curves and 3-D flow patterns

STANFORD
AERONAUTICS &
ASTRONAUTICS

In this example, Q and R are used to study the local flow geometry of a temporally evolving mixing layer

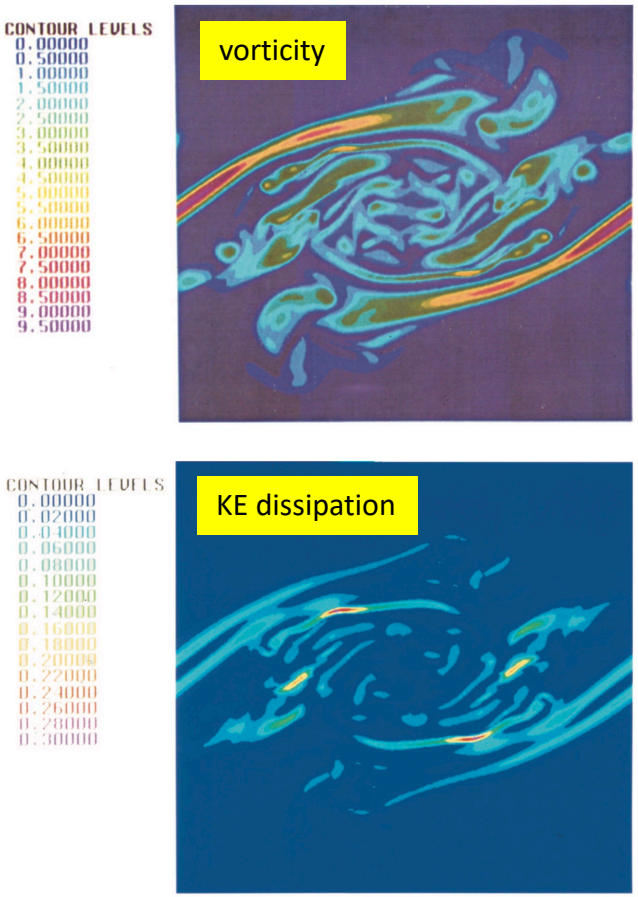

Color plate 1.

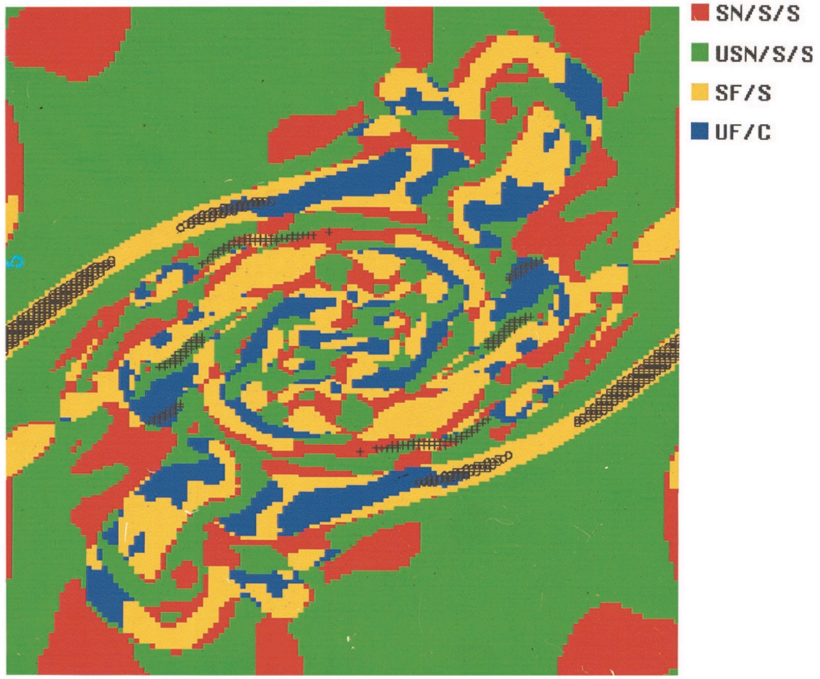

Color plate 2.

This is an efficient, quantitative way to investigate the 3D structure of a turbulent flow.

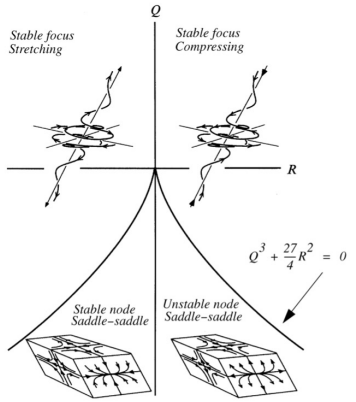

Fig. 3.9. Three-dimensional flow patterns in the plane $P = 0$ (from Reference [3.11]).

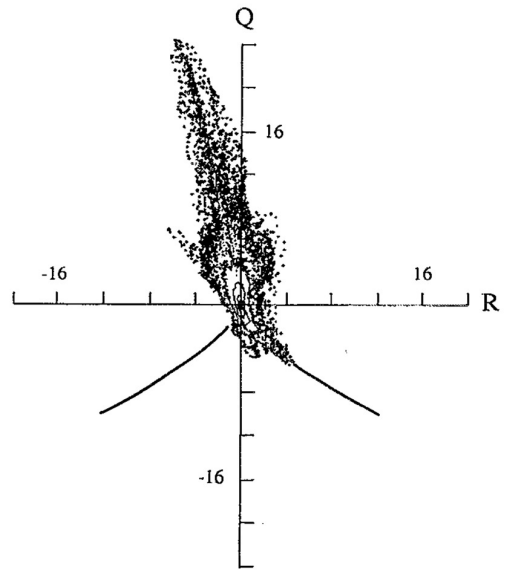

FIG. 2. Number density contour plot of velocity gradient tensor invariants from direct numerical simulation of a plane mixing layer by Moser and Rogers.[8] Dimensionless time $tU_0/\delta=29.8$ where δ is the initial vorticity thickness and U_0 is one-half the velocity difference across the layer. For further details see Ref. 5.

STANFORD AERONAUTICS & ASTRONAUTICS

Use the NS equations to analyze the dynamics of Q and R

Differentiate the NS equations to produce an equation for a^i_j

$$\frac{\partial}{\partial x^j}\left(\frac{\partial u^i}{\partial t} + u^k\frac{\partial u^i}{\partial x^k} + \frac{1}{\rho}\frac{\partial p}{\partial x^i} - \nu\frac{\partial^2 u^i}{\partial x^k\,\partial x^k}\right) = 0. \qquad (11.130)$$

Carrying out the differentiation and applying the continuity equation for incompressible flow, $a^i_i = 0$, leads to

$$\frac{\partial a^i_j}{\partial t} + u^k\frac{\partial a^i_j}{\partial x^k} + a^i_k a^k_j + \frac{1}{\rho}\frac{\partial^2 p}{\partial x^i\,\partial x^j} - \nu\frac{\partial^2 a^i_j}{\partial x^k\,\partial x^k} = 0. \qquad (11.131)$$

Now take the trace of (11.131) to generate the Poisson equation for the pressure:

$$\frac{1}{\rho}\frac{\partial^2 P}{\partial x^i\,\partial x^i} = -a^i_k a^k_i. \qquad (11.132)$$

Equation (11.132) is subtracted from (11.131) to make the pressure term trace-free. The final result is the transport equation for the velocity gradient tensor,

$$\frac{Da^i_j}{Dt} + a^i_k a^k_j - \frac{1}{3}\left(a^m_n a^n_m\right)\delta^i_j = h^i_j, \qquad (11.133)$$

where

$$h^i_j = -\frac{1}{\rho}\left(\frac{\partial^2 p}{\partial x^i\,\partial x^j} - \frac{1}{3}\frac{\partial^2 p}{\partial x^k\,\partial x^k}\delta^i_j\right) + \nu\frac{\partial^2 a^i_j}{\partial x^k\,\partial x^k}. \qquad (11.134)$$

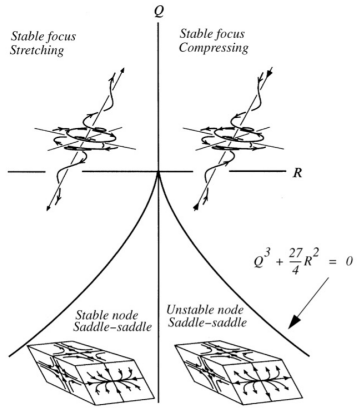

Fig. 3.9. Three-dimensional flow patterns in the plane $P = 0$ (from Reference [3.11]).

$$Q = -\frac{1}{2}a^j_k a^k_j \qquad R = -\frac{1}{3}a^j_k a^k_m a^m_j$$

$$\frac{dQ}{dt} + 3R = -a^i_k h^k_i \qquad \frac{dR}{dt} - \frac{2}{3}Q^2 = -a^i_n a^n_m h^m_i$$

If $h^i_j = 0$ the discriminant is conserved on particle paths.

$$D = Q^3 + \frac{27}{4}R^2$$

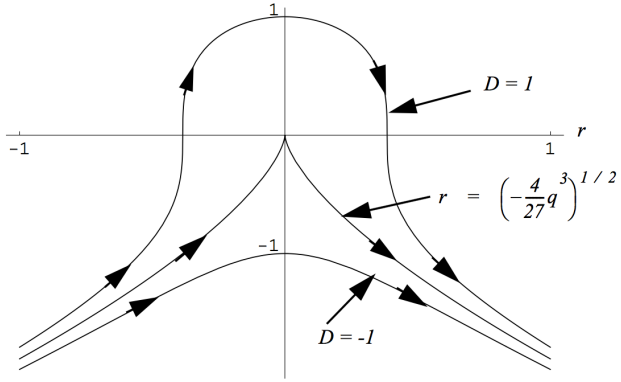

Fig. 6.6. Lines of constant normalized discriminant.

Elliptic curves and 3-D flow patterns

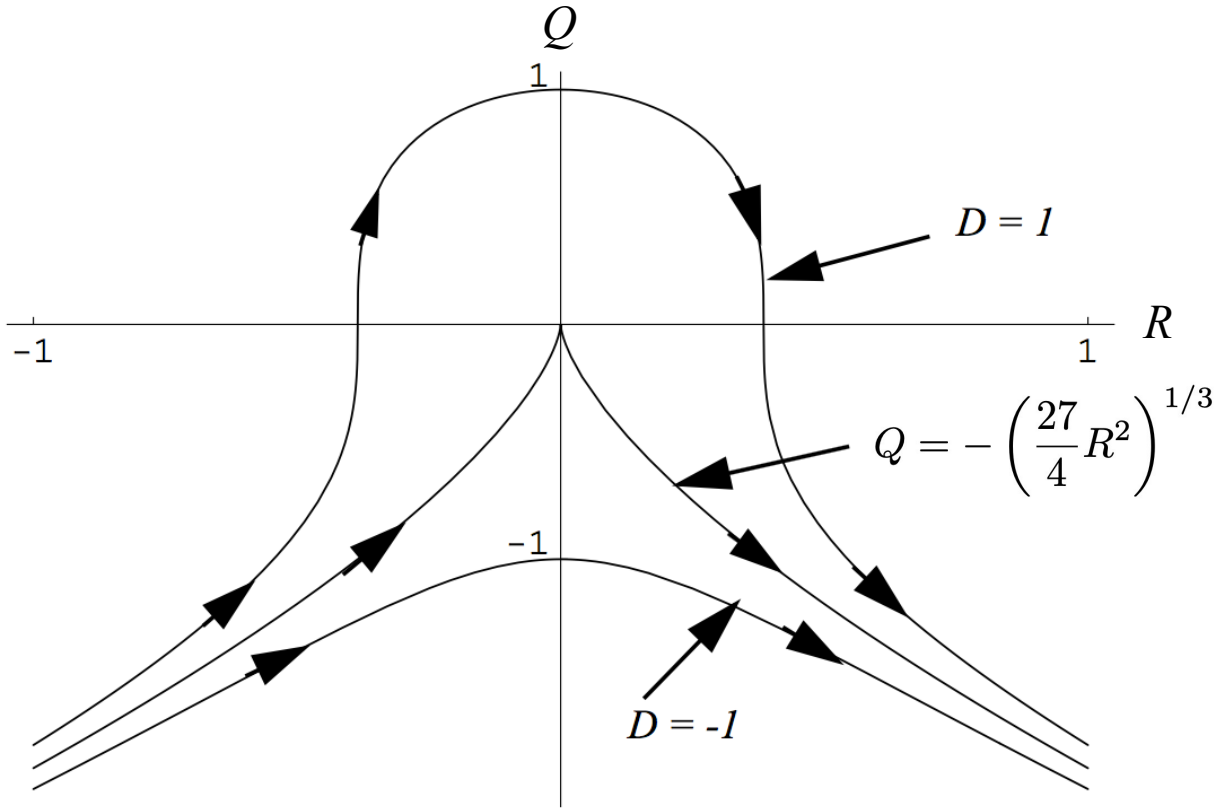

Fig. 6.6. Lines of constant normalized discriminant.

$$D = Q^3 + \frac{27}{4}R^2$$

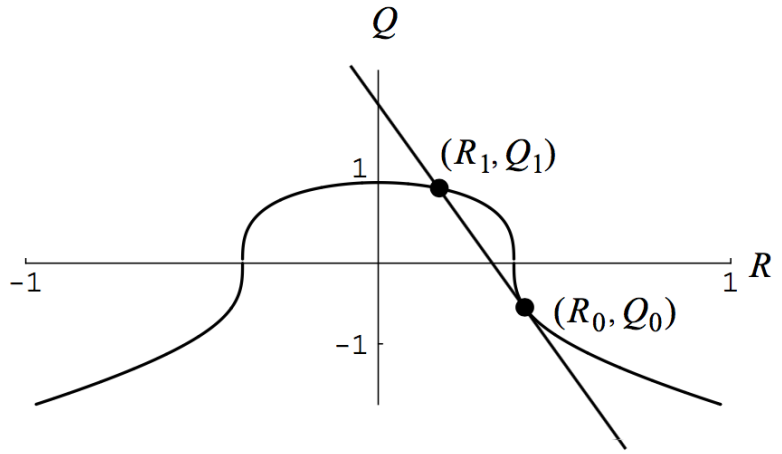

Fig. 6.7. Construction to find rational roots on a curve of constant D.

The cubic discriminant has the same value at both points of intersection in Figure 6.7,

$$Q_1^3 + \frac{27}{4} R_1^2 = Q_0^3 + \frac{27}{4} R_0^2, \tag{6.132}$$

and the straight line is of the form

$$R + aQ + b = 0. \tag{6.133}$$

At (R_0, Q_0) the straight line and line of constant D have the same slope as well as the same coordinates. This is used to evaluate a and b, and the equation of the straight line is determined to be

$$R + \left(\frac{2}{9}\frac{Q_0^2}{R_0}\right) Q + \left(-\frac{2}{9}\frac{Q_0^3}{R_0} - R_0\right) = 0. \tag{6.134}$$

Now evaluate (6.134) at (R_1, Q_1), and use it to replace R_1 in (6.132). The result

is a cubic equation for Q_1, which can be factored as

$$(Q_1 - Q_0)^2 \left(Q_1 + \frac{1}{3}\frac{Q_0^4}{R_0^2} + 2Q_0 \right) = 0. \tag{6.135}$$

Two of the roots coincide with the tangent point. The third root, combined with (6.134), leads to the parameterization

$$\begin{aligned} Q_1 &= -\frac{1}{3}\frac{Q_0^4}{R_0^2} - 2Q_0, \\ R_1 &= \frac{2}{27}\frac{Q_0^6}{R_0^3} + \frac{2}{3}\frac{Q_0^3}{R_0} + R_0. \end{aligned} \tag{6.136}$$

It is clear that if Q_0 and R_0 are rational numbers, then so are Q_1 and R_1. Repeating the chord–tangent construction at the new root leads to a third rational root, and so on.

All the various bifurcations in the topology of the impulsively started round jet occur at rational values of the invariants of the velocity gradient tensor as well as the acceleration gradient tensor.

Acceleration field in the impulsively started jet

When (11.133) is transformed to similarity variables for the round jet, the result is

$$-A^i_j + \left(U_k - \frac{1}{2}\xi_k\right)\frac{\partial A^i_j}{\partial \xi_k} + A^i_k A^k_j - \frac{1}{3}\left(A^m_n A^n_m\right)\delta^i_j = H^i_j, \quad (11.135)$$

where H is the same as (11.134) but expressed in terms of (U^i, P, ξ^i). At a critical point, the convective term in (11.135) is zero, and A and H are algebraically related by

$$-A^i_j + A^i_k A^k_j - \tfrac{1}{3}\left(A^m_n A^n_m\right)\delta^i_j = H^i_j. \quad (11.136)$$

Squaring (11.136) and taking the trace produces

$$Q_H = -\tfrac{1}{3}Q_A^2 + Q_A - 3R_A. \quad (11.137)$$

Cubing (11.136) and taking the trace produces

$$R_H = -R_A^2 - R_A + Q_A R_A - \tfrac{2}{3}Q_A^2 - \tfrac{2}{27}Q_A^3. \quad (11.138)$$

Now switch over, and square (11.138) and cube (11.137) to form the discriminant of the acceleration gradient tensor H: The result is

$$Q_H^3 + \tfrac{27}{4}R_H^2 = \left(Q_A^3 + \tfrac{27}{4}R_A^2\right)(1 + Q_A - R_A)^2. \quad (11.139)$$

A remarkably simple result! A generalization of this procedure is described in [11.27].

We can express the invariants of H in terms of the invariants of M . The result is

$$
\begin{aligned}
Q_H &= 3Q_M - 3R_M - \tfrac{1}{3}Q_M^2 - \tfrac{27}{16}, \\
R_H &= -R_M^2 - \tfrac{9}{4}R_M + 2Q_M R_M - \tfrac{2}{27}Q_M^3 - \tfrac{5}{4}Q_M^2 + \tfrac{9}{4}Q_M - \tfrac{27}{32}, \\
Q_H^3 + \tfrac{27}{4}R_H^2 &= \left(Q_M^3 + \tfrac{27}{4}R_M^2 + \tfrac{27}{4}R_M\left(\tfrac{1}{2} - Q_M\right) - \tfrac{9}{16}Q_M^2\right)\left(R_M - \tfrac{3}{2}Q_M\right)^2.
\end{aligned}
\tag{11.140}
$$

Note that the terms of sixth order in Q_A or Q_M that would be expected when the discriminant of H is formed in (11.139) and (11.140) have canceled. At the off-axis critical point in Figure 11.11, where $R_M = 0$ we find,

$$
\begin{aligned}
Q_H &= 3Q_M - \tfrac{1}{3}Q_M^2 - \tfrac{27}{16}, \\
R_H &= -\tfrac{2}{27}Q_M^3 - \tfrac{5}{4}Q_M^2 + \tfrac{9}{4}Q_M - \tfrac{27}{32}, \\
Q_H^3 + \tfrac{27}{4}R_H^2 &= \tfrac{9}{4}Q_M^4\left(Q_M - \tfrac{9}{16}\right).
\end{aligned}
\tag{11.141}
$$

The trajectory of the critical points of the round jet in the (R_H, Q_H) plane, with the off-axis point parameterized by Q_M as in (11.141), is depicted in Figure 11.12. Four significant points are labeled in these plots:

Point a. This corresponds to the zero-Reynolds-number (Stokes flow) limit of the jet, where there is a single stable node on the jet axis. The invariants of this critical point are

$$\begin{aligned}(R_A, Q_A) &= \left(\tfrac{1}{32}, -\tfrac{3}{16}\right),\\ (R_M, Q_M) &= \left(\tfrac{1}{16}, \tfrac{9}{16}\right),\\ (R_H, Q_H) &= \left(-\tfrac{125}{2048}, -\tfrac{75}{256}\right).\end{aligned} \tag{11.142}$$

Point b. Let the Reynolds number increase. At a critical Reynolds number of 5.5 the jet undergoes a bifurcation to a saddle on the jet axis and a stable node off the axis. The invariants at the bifurcation point are

$$\begin{aligned}(R_A, Q_A) &= \left(\tfrac{1}{4}, -\tfrac{3}{4}\right),\\ (R_M, Q_M) &= (0, 0),\\ (R_H, Q_H) &= \left(-\tfrac{27}{32}, -\tfrac{27}{16}\right).\end{aligned} \tag{11.143}$$

Point c. As the jet Reynolds number increases to infinity, the on-axis critical point moves to infinity and the invariants asymptote to the values given at c:

$$\begin{aligned}(R_A, Q_A) &= \left(\tfrac{27}{32}, -\tfrac{27}{16}\right),\\ (R_M, Q_M) &= \left(\tfrac{1}{8}, -\tfrac{15}{16}\right),\\ (R_H, Q_H) &= \left(-\tfrac{9261}{2048}, -\tfrac{1323}{256}\right).\end{aligned} \tag{11.144}$$

Point d. Above the first bifurcation Reynolds number, the invariants of the off-axis critical point move upward along a straight line until, at a second critical Reynolds number of 7.545, the off-axis critical point turns into a stable node. Thus a starting vortex from the jet is born. The invariants of the off-axis point at this Reynolds number are

$$\begin{aligned}(R_A, Q_A) &= \left(-\tfrac{1}{32}, -\tfrac{3}{16}\right),\\ (R_M, Q_M) &= \left(0, \tfrac{9}{16}\right),\\ (R_H, Q_H) &= \left(\tfrac{27}{2048}, -\tfrac{27}{256}\right).\end{aligned} \tag{11.145}$$

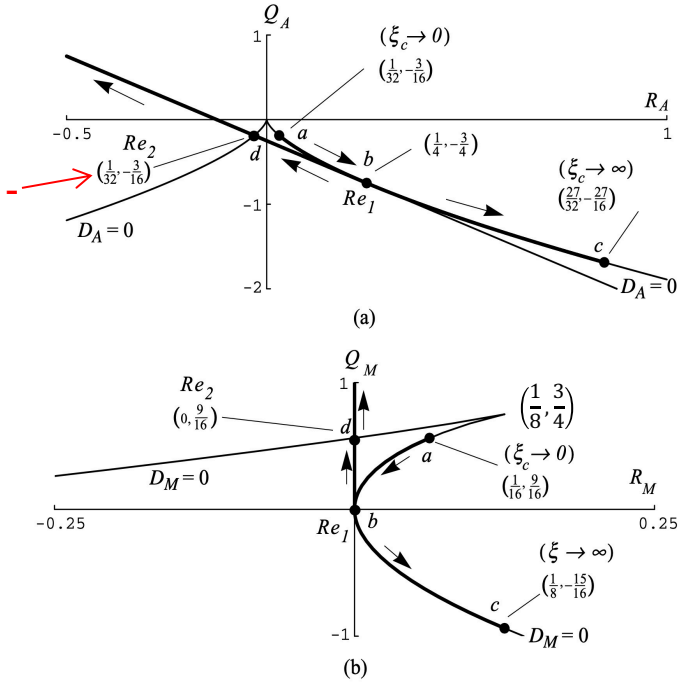

Fig. 11.8. Critical-point trajectories in the round jet: (a) the trajectory in (Q_A, R_A) coordinates at various Re; (b) the same trajectory in (Q_M, R_M).

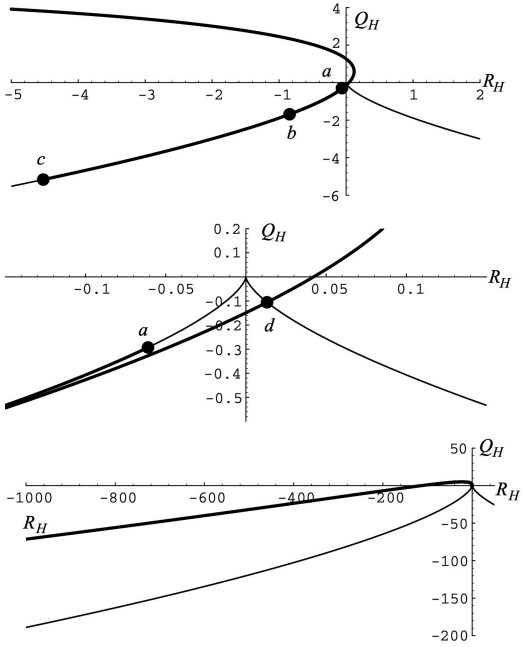

Fig. 11.12. Trajectory of the critical points of the round jet in the (Q_H, R_H) plane at three levels of magnification. Dots indicate several rational roots on the $D_H = 0$ boundary (on-axis critical point) and on the trajectory of the off-axis critical point. The labels a, b, c, and d coincide with the same labels in Figure 11.8.

These results have interesting implications for the limiting behavior of the off-axis critical point, which, eventually closes on the $D_H = 0$, $R_H < 0$ line as $Re \to \infty$. The signs of the discriminant of all three tensors are the same. Thus, if M has complex eigenvalues, so have H and A. This means that the purely viscous, antisymmetric part of H^i_j remains important but diminishes compared to the symmetric pressure-dominated part as the Reynolds number increases. The viscous contribution to the forces at the critical point is never negligible. Finally, the invariants of the on-axis critical point have finite, rational values as the limit $Re \to \infty$ is taken. Few such infinite-Reynolds-number limits are known in fluid mechanics.

Contours of constant discriminant of the acceleration tensor $D_H=Q_H^3 + (27/4)\, R_H^2$

What trajectory in (Q_M, R_M) space would the critical point invariants of the 3D jet follow?

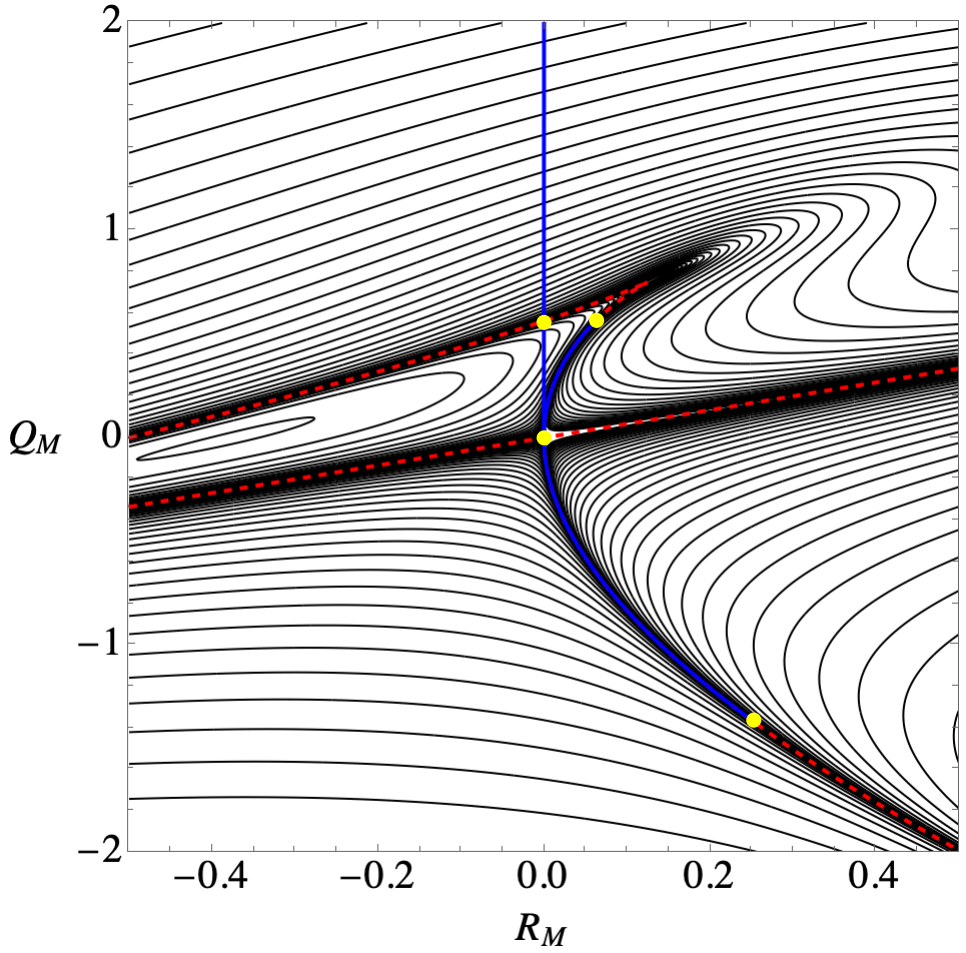

$$Q_H^3 + \tfrac{27}{4} R_H^2 = \left(Q_M^3 + \tfrac{27}{4} R_M^2 + \tfrac{27}{4} R_M\left(\tfrac{1}{2} - Q_M\right) - \tfrac{9}{16} Q_M^2\right)\left(R_M - \tfrac{3}{2} Q_M\right)^2$$

Concluding Remarks

What is the trajectory of the fully 3-D jet in the space of (Q_M, R_M) invariants?

Presumably waves will form and associated with the waves will be 3D critical points, increasing in number as the Reynolds number is increased. What is the trajectory of the flow in the space of invariants, and can the infinite Reynolds number topological limit of the jet be inferred from a moderate Reynolds number computation? Can the onset of 3D flow be induced without permanently introducing a length scale to the flow?

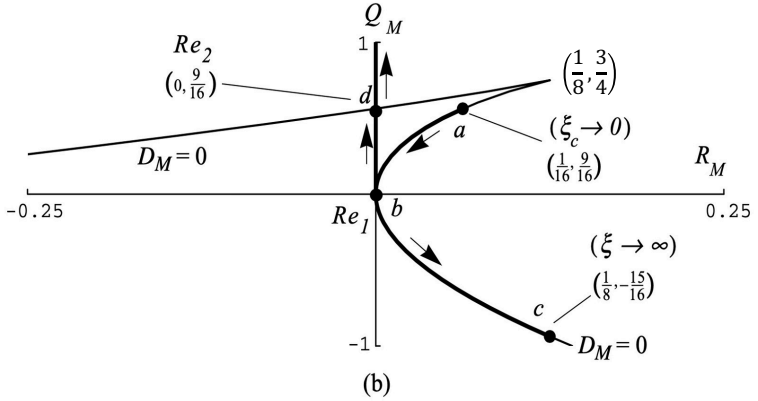

Fig. 11.8. Critical-point trajectories in the round jet: (a) the trajectory in (Q_A, R_A) coordinates at various Re; (b) the same trajectory in (Q_M, R_M).

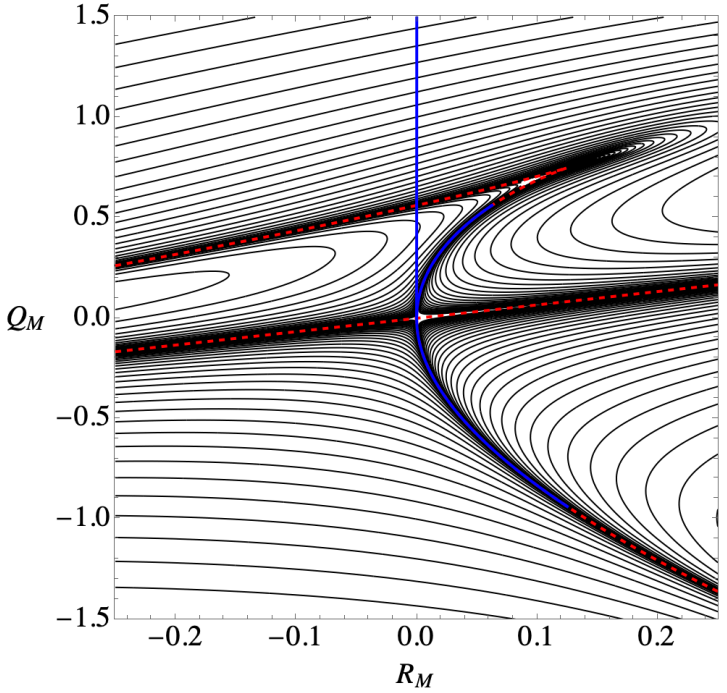

This problem, and perhaps others with k = ½, presents us with a unique opportunity to learn about the fundamentally geometric nature of turbulent flow in the limit of infinite Reynolds number.

STANFORD
AERONAUTICS &
ASTRONAUTICS

Main References

Cantwell, Brian J., *Introduction to Symmetry Analysis,* Cambridge University Press, Cambridge Texts in Applied Mathematics, 2002.

Cantwell, B. J. 1978. Similarity transformations for the two-dimensional unsteady stream-function equation. *J. Fluid Mech*. **85** (2):257–271.

Cantwell, B. J. 1986. Viscous starting jets. *J. Fluid Mech*. **173**:159–189.

Cantwell, B. J. 1981. Transition in the axisymmetric jet. *J. Fluid Mech*. **104**:369–386.

Chong, M. S., Perry, A. E., and Cantwell, B. J. 1990. A general classification of three-dimensional flow fields. *Phys. Fluids A* **2**:765–777.

Cantwell, B. J. 1992. Exact solution of a restricted Euler equation for the velocity gradient tensor. *Phys. Fluids A* ***4 (4)***: 782 - 793.

Cantwell, B. J. 1993. On the behavior of velocity gradient tensor invariants in direct numerical simulations of turbulence. *Phys. Fluids A* ***5 (8)***:2008–2013.

Landau, L. 1944. A new exact solution of the Navier–Stokes equations, *C. R. Acad. Sci. Dokl*. **43**:286–288.

Squire, H. B. 1951. The round laminar jet. *Q. J. Mech. Appl. Math*. **4**:321–329.

Allen, G. A. and Cantwell, B. J. 1986. Transition and mixing in axisymmetric jets and vortex rings. NASA Contractor Report 3893.

Cantwell, B. J. and Allen, G. A. 1983. Transition and mixing in impulsively started jets and vortex rings, in *Turbulence and Chaotic Phenomena in Fluids*, Proceedings of the IUTAM Symposium, Kyoto, Japan, edited by T. Tatsumi.

Cantwell, B. J. 2000. Elliptic curves and three-dimensional flow patterns. *Nonlinear Dynamics* **22**:29–38.

STANFORD
AERONAUTICS &
ASTRONAUTICS

Generalization

Invariants of the velocity gradient tensor are evaluated at every grid point and placed on a cross plot of Q and R.

$$A_{ij}(t) = M_{ij} e^{\int f(t)dt}, \quad \frac{dA_{ij}}{dt} = A_{ij} f(t)$$

$$f A_{ij} + A_{ik}A_{kj} - 1/3(A_{mn}A_{nm})\delta_{ij} = H_{ij}$$

$$Q_H{}^3 + \tfrac{27}{4}R_H^2 = (Q^3 + \tfrac{27}{4}R^2)(R + fQ + f^3)^2$$

For the round jet the negative slope $f = -1$

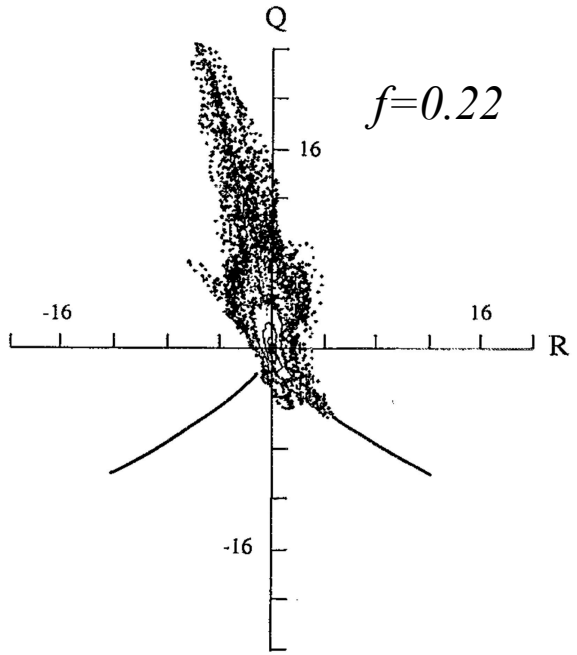

FIG. 2. Number density contour plot of velocity gradient tensor invariants from direct numerical simulation of a plane mixing layer by Moser and Rogers.[8] Dimensionless time $tU_0/\delta = 29.8$ where δ is the initial vorticity thickness and U_0 is one-half the velocity difference across the layer. For further details see Ref. 5.

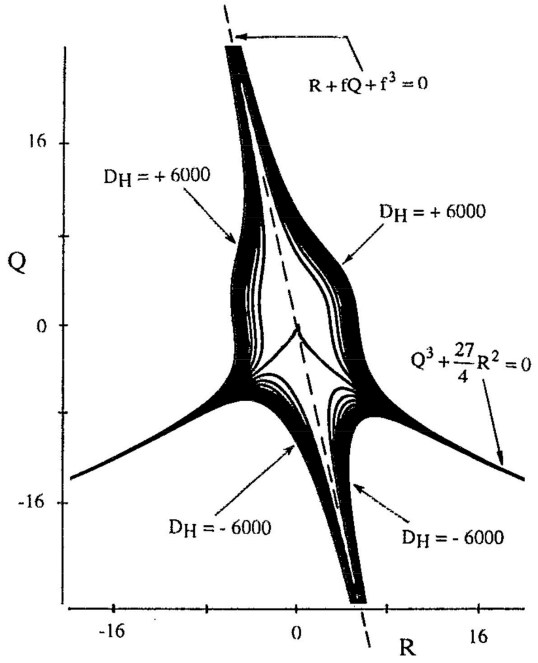

FIG. 3. Contours of constant $D_H = Q_H^3 + \frac{27}{4}R_H^2$ with $f(t) = 0.22$ [see Eq. (16)].

Cantwell, B. J. 1993. On the behavior of velocity gradient tensor invariants in direct numerical simulations of turbulence. *Phys. Fluids A* ***5 (8)***:2008–2013.

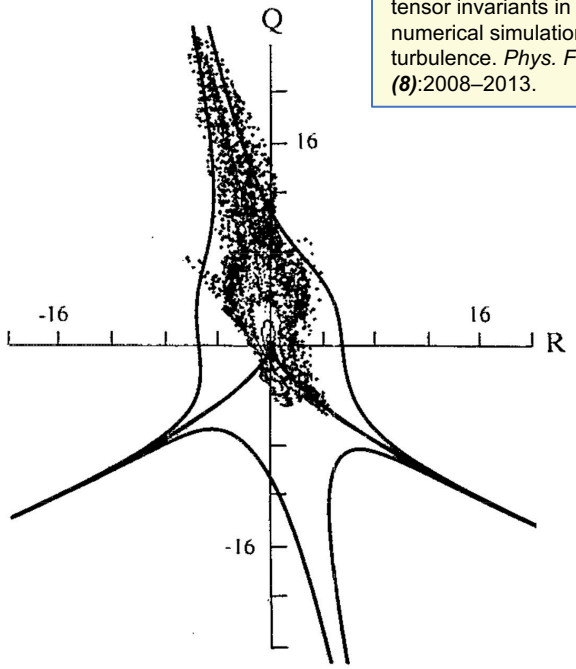

FIG. 4. Data from Fig. 2 superimposed on maximum, minimum, and zero contours of Fig. 3.

Previous numerical computations

Allen, G. A. and Cantwell, B. J. 1986. Transition and mixing in axisymmetric jets and vortex rings. NASA Contractor Report 3893.

Finite difference computation on a 60x60 mesh on a CDC7600

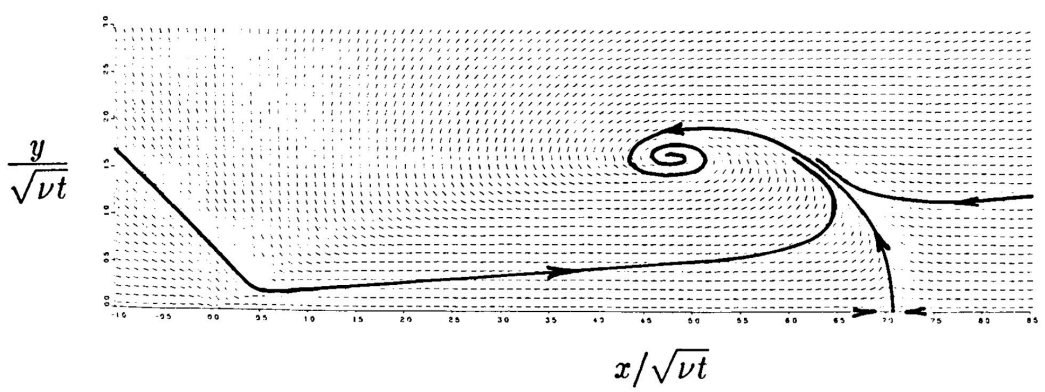

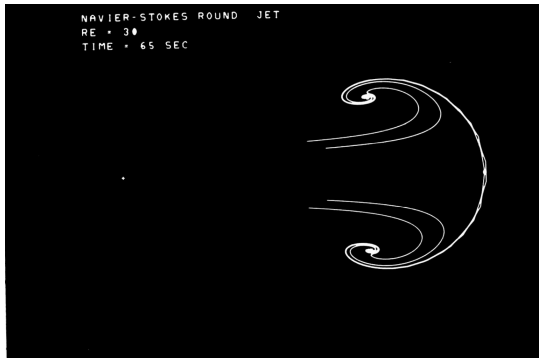

S. K. Stanaway, B. J. Cantwell, P. R. Spalart 1988. A Numerical Study of Viscous Vortex Rings Using a Spectral Method. NASA Technical Memorandum 101041.

Spectral computation of viscous interacting vortex rings using vector spherical harmonics